Adrian W. Brink – Mechanical Engineer

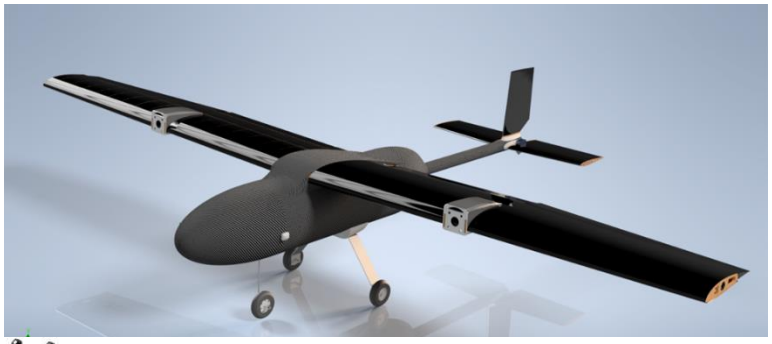

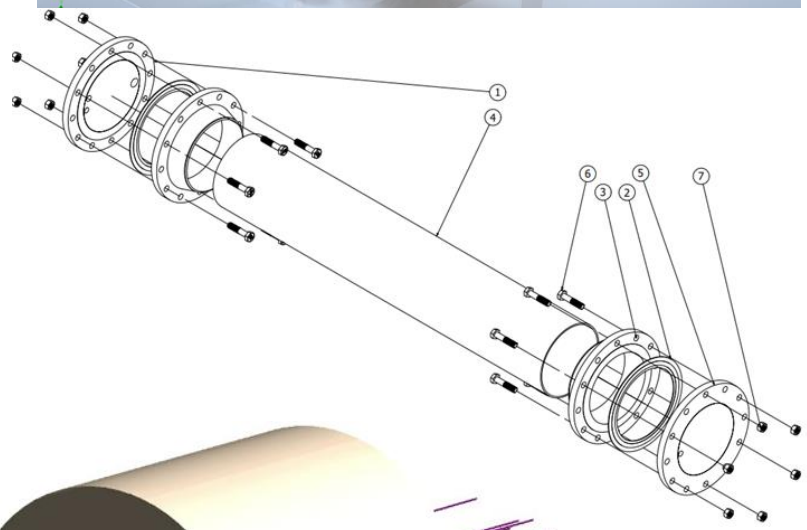

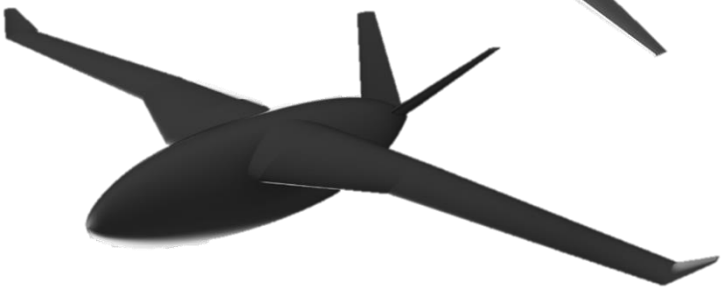

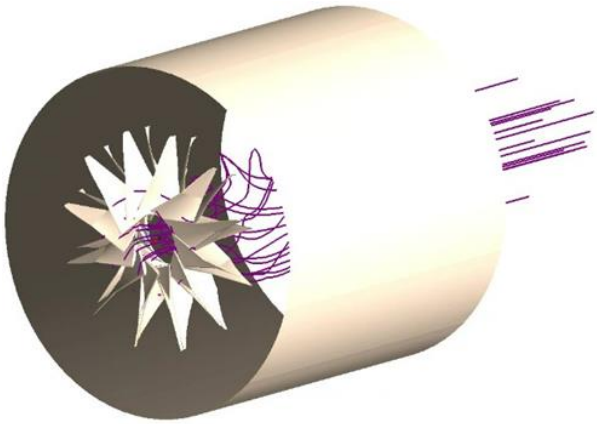

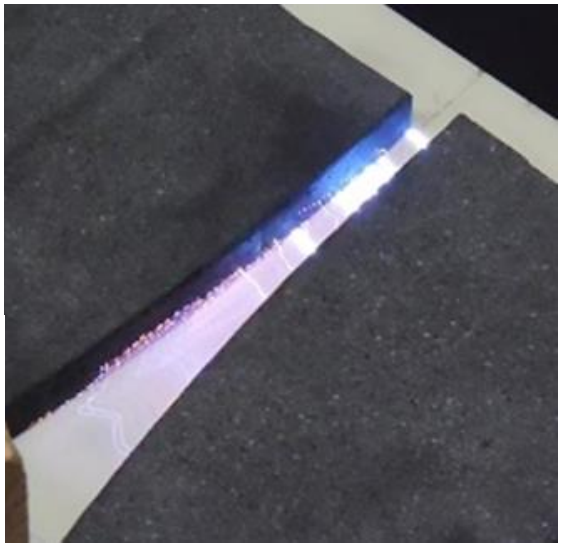

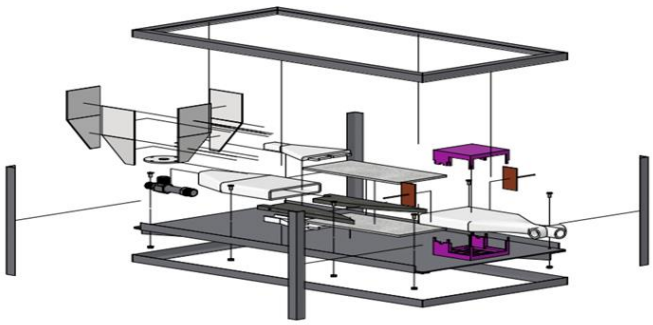

Table of Contents

2019 - 2020 AIAA Design Build Fly (DBF)

My first year as a student I worked with the Raider Aerospace Society (RAS) to develop a design for a small-scale aircraft for competition in that year's DBF. I was responsible for the development of the tail wing section, electric motor mounting system, fuselage structure and loading system, as well as serving as the manufacturing lead while building. I developed 3D models based on , performed structural analysis, composite layup design, and iterative design changes to solve problems which arose during manufacturing.

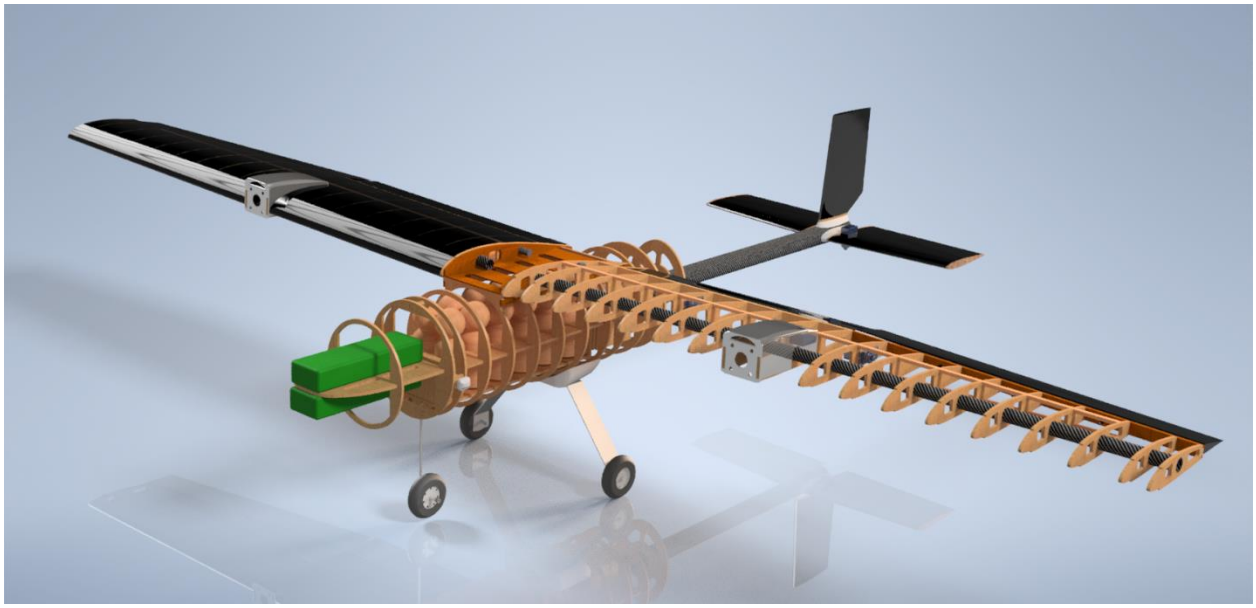

The internal structure of the plane was made from two types of wood in the wing and fuselage sections. The wings were constructed from poplar wood and cut to shape using a laser cutter, then placed and glued form a rigid wing which could withstand the bending moments placed on the structure. The fuselage section however used a carbon fiber hull construction as its primary structural component which allowed for the use of lighter materials for the internal structure, in this case balsa wood, which could perform a mission focused role and allow for faster loading.

The carbon fiber composite structure was formed using an Out of Autoclave vacuum bag forming technique with the aid of a 3D printed mold, with a water based release agent applied, to apply a layup consisting of four layers and two fabric types of carbon fibers (a twill weave and three layers of mono-directional fabric which laid in orientations according to principal stresses acting on the structure in flight).

2020 - 2021 AIAA Team Aircraft Design

The following is a collection of sections from the proposal submitted to the 2021 AIAA Team Aircraft Design competition the year that I served as the Project Manager and Propulsion Systems lead. I was responsible for systems integration and development of a full system CAD model that could be used for analysis and for the creation of figures in the report. I also performed design and analysis to select propulsion systems for the proposed aircraft. The following are sections from the report which I wrote.

AIAA 2020 – 2021 Undergraduate Team Design RFP Austere Field Light Attack Aircraft

Final Design Report – Project Aquila

Adrian Brink, Eric Gardea, Liam Hunt, Hassan Khalil, Dylan Lee, Sebastian Valbuena

Raider Aerospace Society – PEGASUS Team

Texas Tech University, Lubbock, Texas 79406

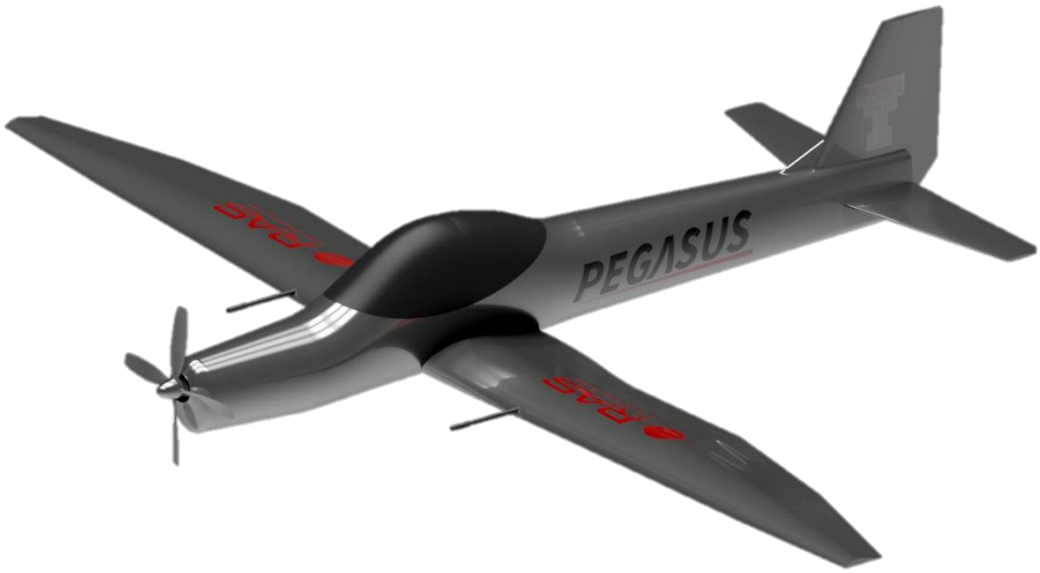

Faculty Advisor: Andrew Mosedale

Department of Mechanical Engineering

Texas Tech University, Lubbock, Texas 79406

Date of Submission: May 14, 2021

Executive Summary

With an aging fleet of aircraft in service in the United States Air Force and Navy, there is a need for more advanced and capable aircraft that can take on the challenges of a changing battlefield. Increasingly, there is a need for smaller close air support aircraft that can support ground troops and be versatile in the type of mission they are capable of accomplishing. This report will document a preliminary design for a Light Attack Aircraft capable of utilizing austere fields as requested by the AIAA Undergraduate Team Aircraft Design Challenge.

The formal requirements of the RFP stipulate that the design shall be capable of operating off austere fields, defined as a runway with a 50 ft obstacle within $\leq$ 4,000 ft and a density altitude up to 6,000 ft, and a semi-prepared runway surface such as grass or dirt surfaces with a California Bearing Ratio of 5. The aircraft must be capable of carrying a payload of 3000 lbs. in armament and have an integrated gun for engaging ground targets as part of its offensive capabilities. The aircraft must also reach a service life of 15,000 hours over the course of 25 years, a service ceiling of $\geq$ 30,000 ft, and be able to accommodate two crew members with zero-zero ejection seats for crew survivability. This report covers the preliminary design and sizing of the Project Aquila aircraft.

Figure 1 Project Aquila Plane

V. Introduction

The phase out of very successful military aircraft such as the A-10 calls for a new generation of light attack aircraft to fill that role on a continuously changing battlefield. As determined by the AIAA RFP, a light attack aircraft capable of utilizing austere fields, and accommodating two crew members is to be designed. The RFP also stated that the design objective is to design a “best value” aircraft that can perform essential military functions without becoming terminally expensive, hard to produce, or difficult to maintain.

VI. Concept of Operations

The major requirements laid out in the RFP are listed in Table 2 [1]. The requirements for payload, range, service life and crew configuration were the most influential on the final design, and priorities such as combative hardware were made to fit into these constraints.

Table 2 RFP Requirements

Requirement	Comments
Austere Field Performance	Takeoff and landing over a 50ft obstacle in < 4000 ft. Semi-prepared runways with California Bearing Ratio of 5.
Payload	3000 lbs. of armament
Integrated Gun	Must have combative hardware for engaging ground targets
Service Life	15,000 hours over 25 years
Service Ceiling	>30,000 ft in altitude
Crew	Two crew members, zero-zero ejection seats equipped
Survivability [O]	Consideration of craft and crew mission survivability
Additional Combative Hardware [O]	Provisions for carrying/deployment of additional weapons, 500 lbs. max of bombs.

In addition to the requirements set out in Table 2 there are two differerent service missions the design must be capable of fulfiling.

A. Design Mission

The first mission describes the operation of a standard combattive flight, including a full payload and a set of manuvers which occupy a certain period of time, and a certain amount of additional potential mission which must be accounted for in fuel reserves. This mission profile is desrcibed descriptively in Table 3 and visually in Figure 3 with information from the RFP [1].

Table 3 Design Mission Profile

1	Warmup / Taxi	5 minutes
2	Take off	Austere field, 50 ft obstacle, ≤ 4,000 ft
3	Climb	To cruise altitude, ≥ 10,000 ft; with range credit
4	Cruise	100 n miles
5	Decent	To 3,000 ft; no range credit; completed within 20 minutes of the initial climb
6	Loiter	On station, four hours, no stores drops
7	Climb	To cruise altitude, ≥ 10,000 ft; with range credit
8	Cruise	100 n miles
9	Descent / Landing	To Austere field, 50 ft obstacle, ≤ 4,000 ft
10	Taxi / Shutdown	5 minutes
11	Reserves	Sufficient for climb to 3,000 ft and loiter for 45 minutes

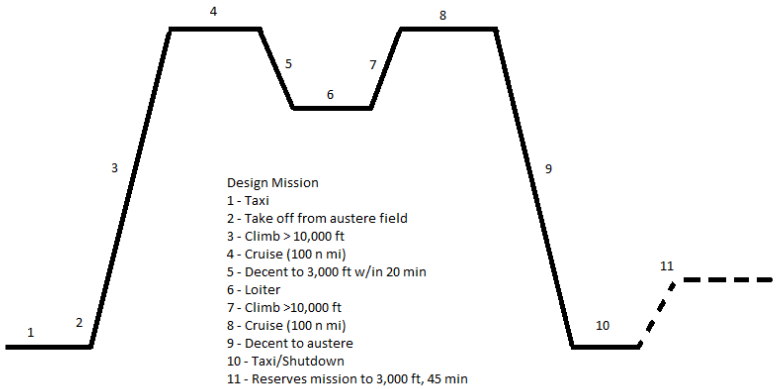

Figure 2 Design Mission Profile

B. Ferry Mission

The aircraft design was also analyzed for a long-range ferry mission which includes a 60% payload and full crew, with the mission profile as laid out in below.

Table 4 Ferry Mission Profile

1	Warmup / Taxi	5 minutes
2	Take Off	Austere field, 50 ft obstacle, ≤ 4,000 ft
3	Climb	To cruise altitude; with range credi
4	Cruise	At best range speed / altitude (≥ 18,000 ft), 900 n mi
5	Decent / Landing	To austere field over 50 ft obstacle in ≤ 4000 ft
6	Taxi / Shutdown	5 minutes
7	Reserves	Sufficient for climb to 3,000 ft and loiter for 45 minutes

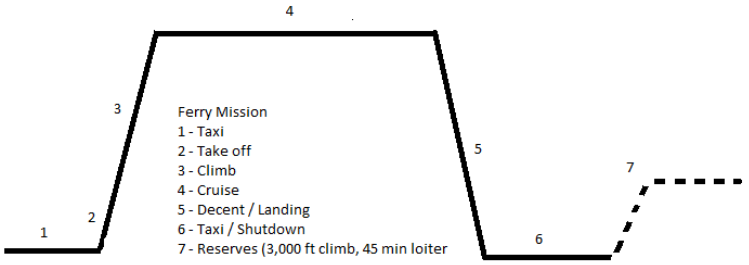

Figure 3 Ferry Mission Profile

VII. Sizing Analysis

A. Similarity Analysis

To gain some perspective on the specification requirements for a light attack aircraft, three light attack airplanes were studied, which were the AT-29, AT-6, and AT-802U. The most important characteristics to analyze for the aircraft were the empty weight, fuel weight, and range, since it is imperative that the aircraft be light weight and be capable of flying the required mission range.

Table 5. Aircraft Comparison Chart

Aircraft	Empty Weight (lb)	Fuel Weight (lb)	Range (nmi)
AT-29	7000	2727	1797
AT-6	5890	2908	1985
AT-802U	12700	6000	2200

The required ferry range was 900 nm, therefore all the aircrafts could easily operate the mission. Since weight and cost needed to be light, the AT-29 and AT6 empty and fuel weights were ideal for a light attack aircraft and were chosen as reference planes for our design.

B. Trade Studies

A trade study was done on light attack aircraft currently on the market and the main objective was to reduce weight, which would reduce the cost and make the plane easier to manufacture and maintain. To ensure the plane was likely to meet this goal, specification limits were determined from the trade study, which were empty weight, maximum take-off weight, armament, max G loading, length, wingspan, and height. These values were determined and put into table #, which were used for the initial design and amended in the final design.

Table 6. Initial Specification Parameters

Empty Weight (lb)	6000
MTWOW (lb)	12000
Armament (lb)	3000
Max G Loading (+,-)	7, 2
Length (ft)	35
Wing Span (ft)	37
Height (ft)	10

VIII. Configuration

A. Design Morphology

The aircraft configuration was initially designed to maximize the space for the crew and internal storage, as well as accommodate space for the engine and front landing gear while adhering to a “best value” objective and other design consideration outlined in the AIAA RFP [1]. One of the main obstacles of this challenge is the necessity of

consistent performance on short and unfinished runways which leave little room for error on both take off and landing. This led to the prioritization of a configuration that allows for aggressive take off angles to maximize the agressiveness the pilot can use when taking off from austere fields.

This line of consideration led to a configuration similar to that of aircraft adapted and modified to combat purposes from small commercial crafts which tend to be used in agricultural settings that utilize these same types of airstrips. This approach led to an analysis of these aircraft through trade studies and eventual iterations on the design which maximized the final design's ab

After the initial set of trade studies and sizing analysis the first 3D model of the aircraft was created using OpenVSP parametric modeling software in order to rough out the desired dimensions and profiles, which resulted in the model shown in Figure 5.

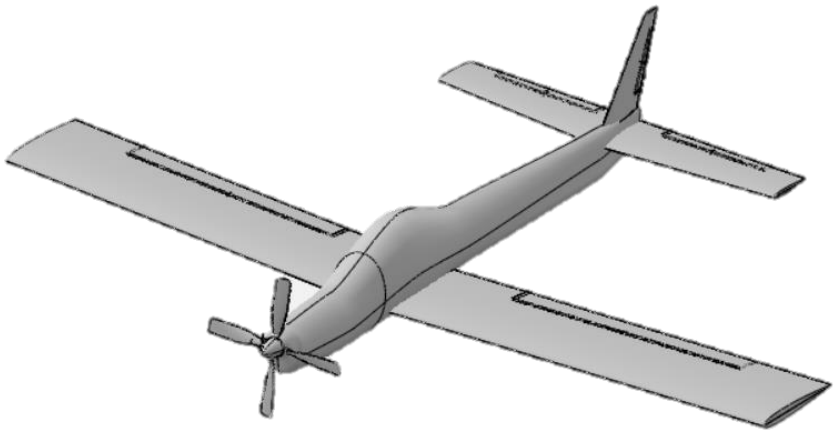

Figure 4 Project Aquila Initial 3D Model

Following the initial model, a wing optimization was run using Aeolus ASP using known ranges of environmental characteristics. Continued iterations using computationally guided design progressed to the final 3D model shown in Figure 6, and is the culmination of the full iterative computational design process.

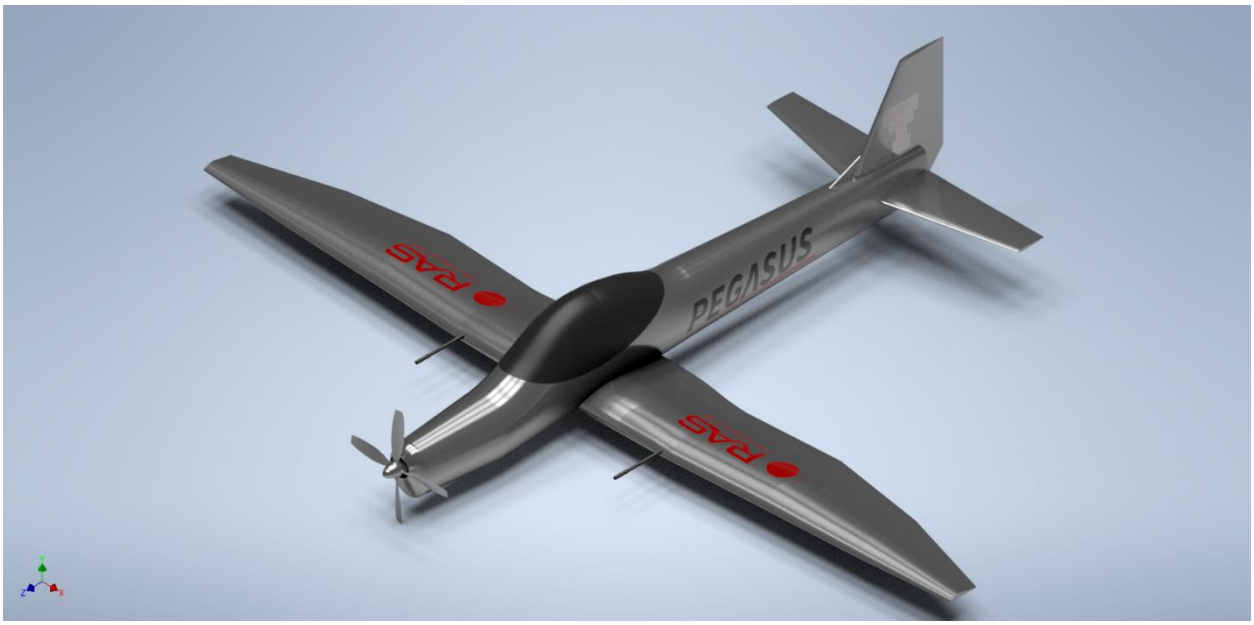

Figure 5 Project Aquila Final 3D Model

B. Landing Gear

Landing Gear is especially important to the design of this aircraft because it is meant for very adverse conditions on austere fields where takeoffs and landings are short and the airstrip material is not always reliable. This design uses a wing/fuselage junction to house the landing gear, allowing for more space for proportunally large and strong gear for the size of the aircraft. The front wheel is designed to be capable of steering the aircraft while in taxi and takoff/landing.

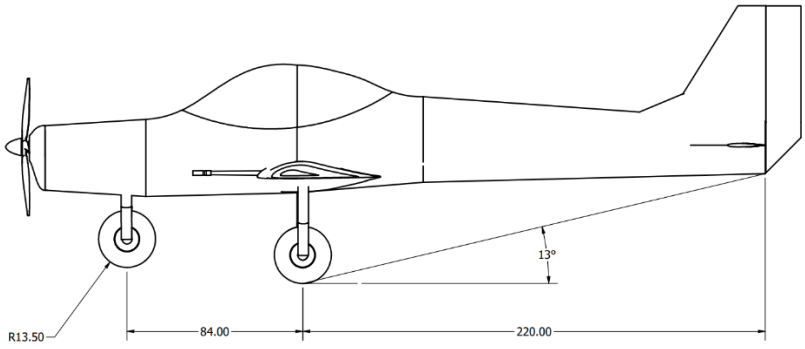

Figure 6. Landing Gear Side View

The landing gear design allow for a break away angle of 13 degrees, allowing the pilot to be more aggressive with the way they manuver the aircraft when taking off on short runways. This manuverability is paired with a wide stance for the rear two wheels to offer high stability and counter the rough conditions of austere fields.

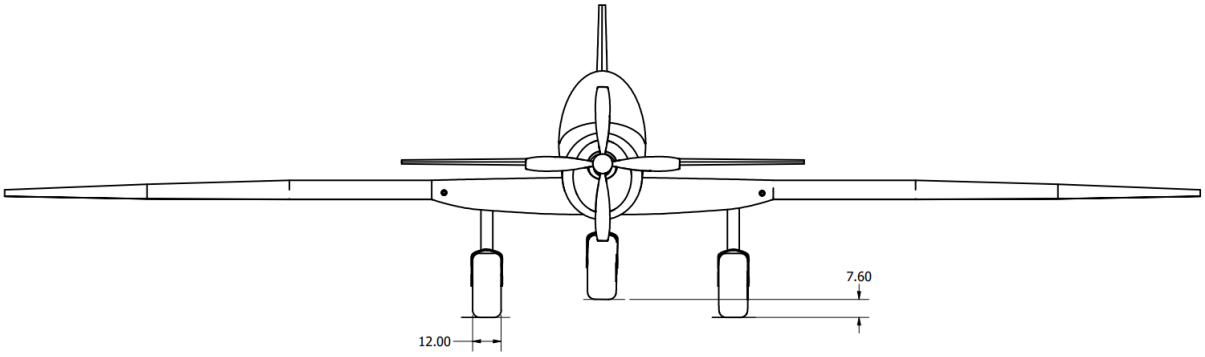

Figure 7. Landing Gear Front View

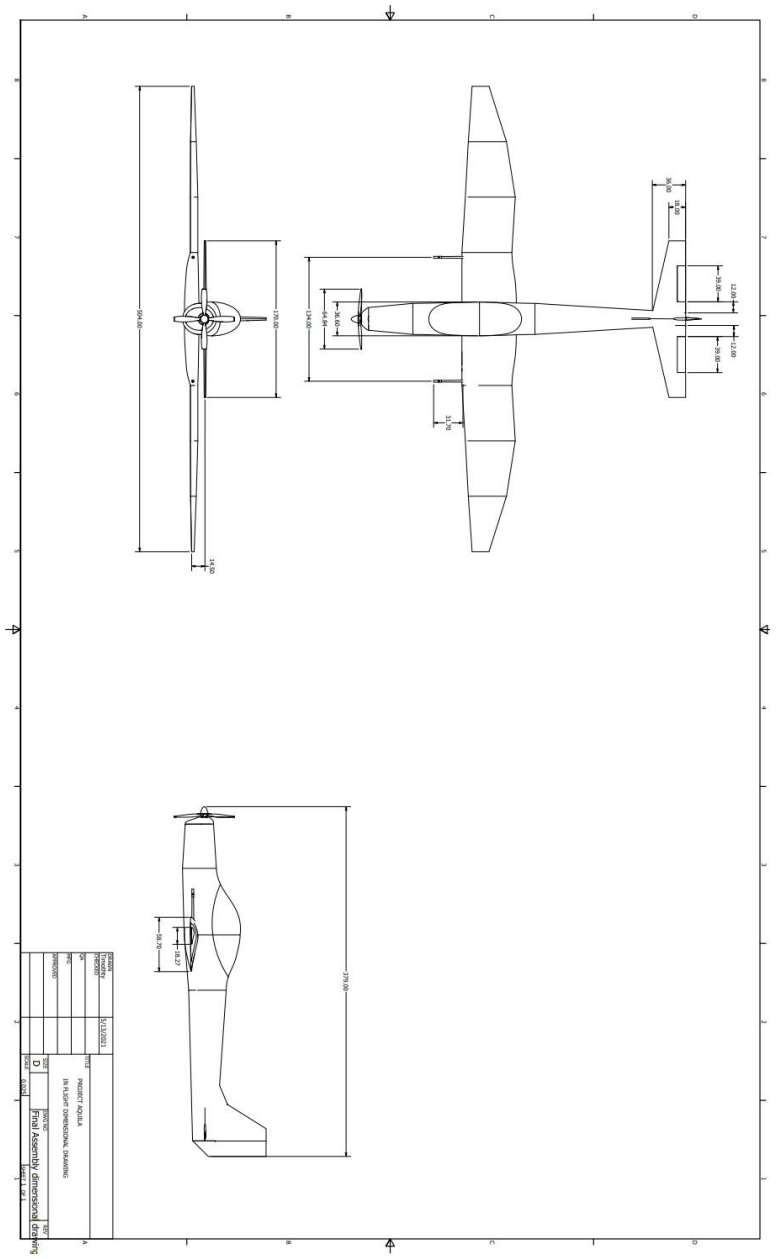

Figure 8. Dimensional Drawing

IX. Propulsion

A. Selection Approach

It was decided for the aircraft that the powerplant would be procured from a market available production engine. This not only saves resources otherwise spent on research and development of a new engine, but also eliminates the production cost of manufacturing a purpose-built engine solely for the design. Several contender models were selected for consideration based on their established use in similar aircraft or from a reputable company's contemporary line. Engines from these sources would have proven reliability and represent the best performance per cost.

Regarding engine possibilities, there were several metrics used in comparing potential selections. Primary concerns were for engine horsepower, unit cost, weight, and fuel consumption. Other, lesser factors considered were engine time-before-overhaul, dimensions, maintenance complexity, ideal operating altitude, and ideal operating speed. Based on trade studies the aircraft would require around 800 equivalent shaft horsepower. Once this power was reached, cost, weight, and fuel consumption would look to be minimized.

B. Trade Studies

A turboprop engine was chosen as the most reasonable engine type for the aircraft's purpose. The engine would need relatively high efficiencies at its cruising altitude of >10,000 ft, but also have adequate performance beneath that altitude for CAS operations. The average speed at this lower altitude would be around 345 mph as supported in the requirements of the 1970 UAFS A-X RFP for a ground attack aircraft [2]. Turbofans for this project's design were eliminated relatively early for their large size, and high ideal operating speed and altitude [3]. Turbojets were also eliminated, as their increasing efficiency with very high speed and very high altitude was not a behavior sought after. Additionally, turbojets had very high fuel consumption, low throttle response times, and low accelerations [4]. The last two points were especially troubling considering the low altitude, low speed nature of the aircraft's operation.

Piston engines tend to lose efficiencies starting from 7,000 feet [5] while turboprops do not reach efficiency until above 18,000 feet [6]; however, with regard to engine size, planes with take-off weights greater than 6,000 lb, found turboprops to be more efficient [5]. Additionally, turboprops have higher power-to-weight ratios and longer time-to-overhaul than piston engines [6]. It was for these reasons that a turboprop engine was selected as the powerplant of the design.

Several candidates for a light attack role were selected to serve as a technological starting point and comparison baseline for the design. The United States Air Force's 2009 Light Attack/Armed Reconnaissance (LAAR) program required many similar requirements in their request for information as this project; thus, many of the demonstrator entries were of particular interest. From within the contenders of the LAAR program, it was noted that several models of turboprop engines were relatively popular and were used in multiple aircraft similar in purpose to this design. These engines are listed below:

Walter M601	as seen in: PZL-130TM Orlik, Dornier Do 28 G.92, Ayres Thrush 510G
Honeywell TPE331	as seen in: Short Tucano T1, Beech B100 King Air, Gen. Atomics MQ-9 Reaper
Pratt-and-Whitney PT6A	as seen in: Embraer EMB 314 Super Tucano, T-6A Texan II, TAI Hürkuş

These models were extensively used in a variety of applications and had proven records of reliability and performance. It was thus from these three that a selection of variants were pulled for comparison and ultimately selection.

C. Serviceability

Several engine series were chosen for selection. Most were currently in use in other aircraft while others were middle-ground versions in production from the manufacturer. Variant selection was also limited by information available.

Engine	Manufacture	Shaft HP	Dry Weight (lb)	Power-to-Weight (hp:lb)	Specific Fuel Consumption (lb/hp/hr)	Unit Cost (USD)	Engine Life (Time-Before-Overhaul) (hr)
M601D-1	General Electric	740	434	1.70:1	0.648	550,000	3000
M601E-11	General Electric	705	394	1.79:1	0.654	570,000	3000
TPE331-1	Honeywell	665	336	1.98:1	0.611	560,000	5400
TPE331-2	Honeywell	715	336	2.13:1	0.621	560,000	5400
TPE331-10	Honeywell	980	385	2.55:1	0.534	565,000	6000
TPE331-11	Honeywell	1020	400	2.55:1	0.530	590,000	6000
TPE331-12	Honeywell	1151	415	2.77:1	0.523	600,000	6000
PT6A-25C	Pratt-and-Whitney	750	335	2.24:1	0.595	720,000	3000
PT6A-42	Pratt-and-Whitney	850	403	2.11:1	0.601	775,000	3000
PT6A-64	Pratt-and-Whitney	700	454	1.54:1	0.703	715,000	3000
PT6A-68	Pratt-and-Whitney	1250	572	2.19:1	0.540	855,000	4500

Table 7. Engine Candidates

A simple linear metric evaluation was used to carry out engine comparison. For each column, the values to be compared were divided into 4 distinct ranges: red, orange, yellow, and green. Each of the ranges was given a simple score of 1, 2, 3, or 4 respectively. The better a specific value was relative to the entire range of the data determined what score it received. Once all the columns had been compared, the scores were summed and compared.

Engine	Shaft HP	Dry Weight (lb)	Power-to-Weight (hp:lb)	Specific Fuel Consumption (lb/hp/hr)	Unit Cost (USD)	Engine Life (Time-Before-Overhaul) (hr)	Total Points
M601D-1	740	434	1.70:1	0.648	550,000	3000	11
M601E-11	705	394	1.79:1	0.654	570,000	3000	12
TPE331-1	665	336	1.98:1	0.611	560,000	5400	17
TPE331-2	715	336	2.13:1	0.621	560,000	5400	16
TPE331-10	980	385	2.55:1	0.534	565,000	6000	22
TPE331-11	1020	400	2.55:1	0.530	590,000	6000	21
TPE331-12	1151	415	2.77:1	0.523	600,000	6000	21
PT6A-25C	750	335	2.24:1	0.595	720,000	3000	15
PT6A-42	850	403	2.11:1	0.601	775,000	3000	13
PT6A-64	700	454	1.54:1	0.703	715,000	3000	7
PT6A-68	1250	572	2.19:1	0.540	855,000	4500	15
Points	4		3		2		1

Table 8. Engine selection metrics chart

From the comparison, it can be seen that the engines best fulfilling the most primary metrics are the TPE331 models, series 10-12. Furthermore, the series 10 engine extends slightly further with a similar power-to-weight ratio but cheaper unit price.

D. Engine Selection

Supported by the metric analysis table in the previous section (Table [8]), the Honeywell TPE331-10 turboprop engine was chosen as the powerplant of the design. The design represented the required power output with a high power-to-weight ratio and engine life without incurring unnecessary cost. While losing the ease of repair available from Pratt-and-Whitney's patented reverse flow inlet configuration [7], it was decided that the combined lower unit price and lower over-haul cost [8] of the Honeywell engine offset this.

E. Engine Characteristics

The engine to be used in the aircraft is a Honeywell TPE331-10 turboprop. It has a unit cost of [around $500,000] with a time-before-overhaul of 6000 hours [9].

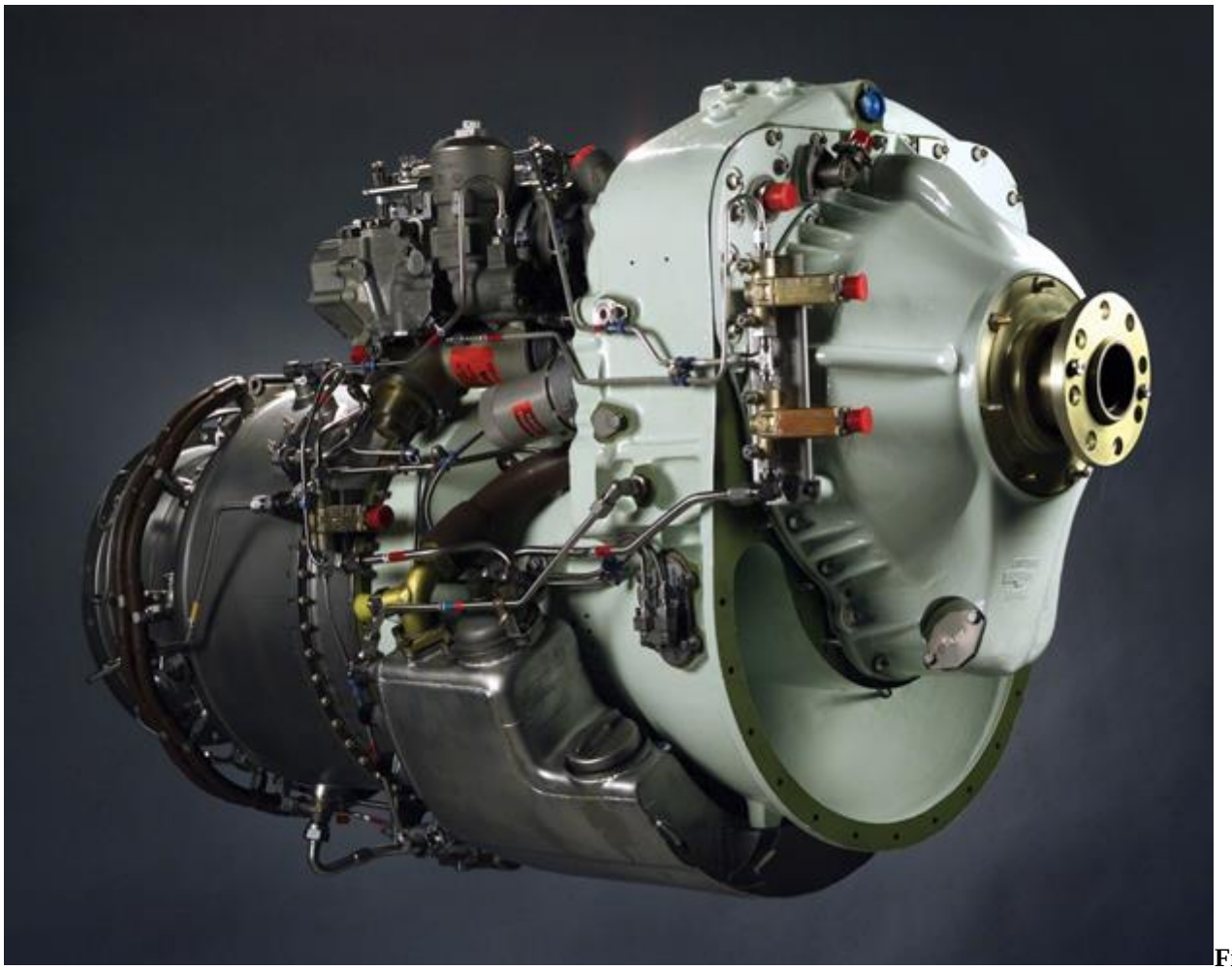

Figure 9. TPE331 Engine [10]

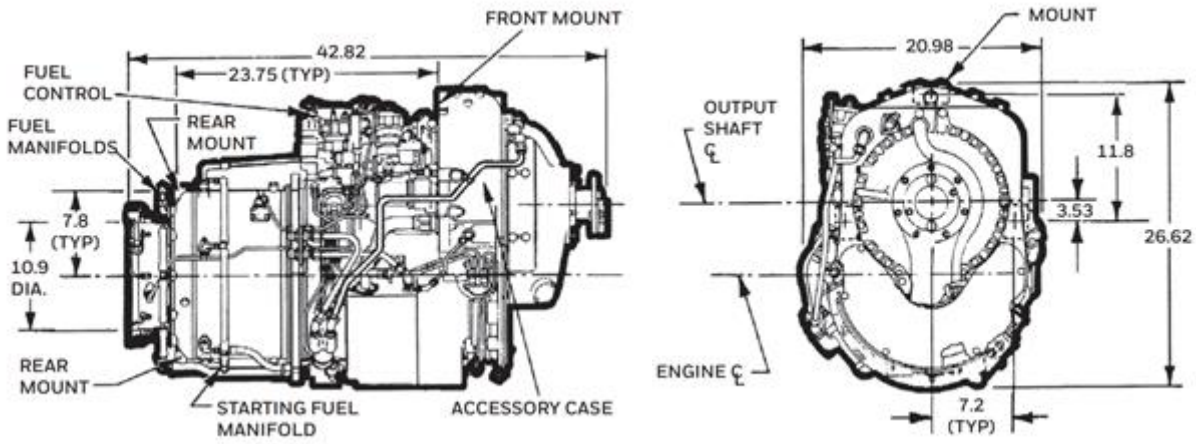

Figure 10. Dimension diagram of TPE331-10 [98]

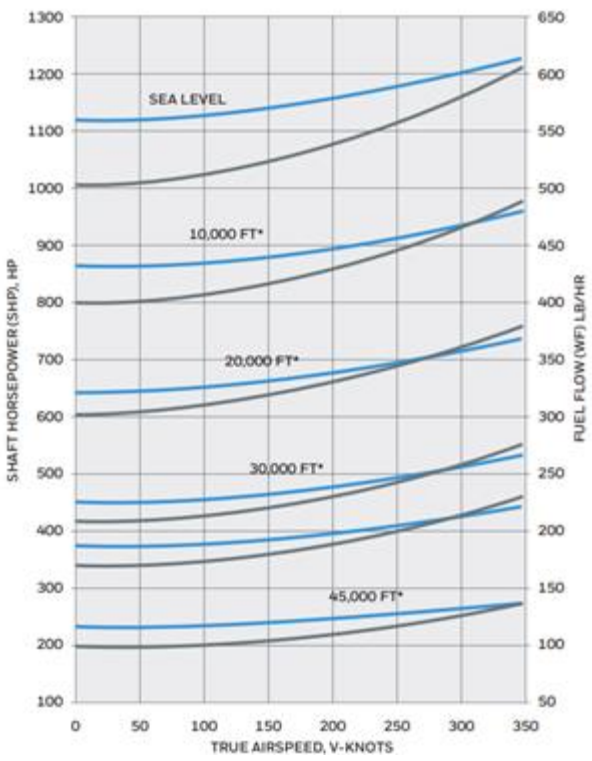

Power output:	shp shp (thermo) eshp eshp (thermo)	940 1,000 944 1,045
ESFC:	0.534	
RPM:	gas gen shaft output	41,730 2,000 (cw from rear) 1,591 (ccw from rear)
Weight:	385 lb	
Pressure ratio:	10.55	
Airflow:	7.7lb/sec	
Fuel:	Jet A, Jet B, Jet A-1, JP-8, JP-1, JP-4, JP-5, JP8+100	
Oil	Mil-L-23699B, Mil-L-7808, Type I/ Type II	
Electrical:	24 vdc,16.2 amp (max)	
(Demonstrated) Start capability:	SL–30,000 ft. No minimum O.A.T. to + 55°C	
(Demonstrated) Operational limits:	SL–45,000 ft. No minimum O.A.T to + 55°C	
Compressor bleed:	high pressure 10% (max)	

*Available in cw and ccw

Figure 11. Performance data of TPE331-10 [98]

For design, simulation, and analysis a model of the engine was created. This would assist in sizing the nose of the aircraft as well as determine the placement of the foremost ribs for mounting.

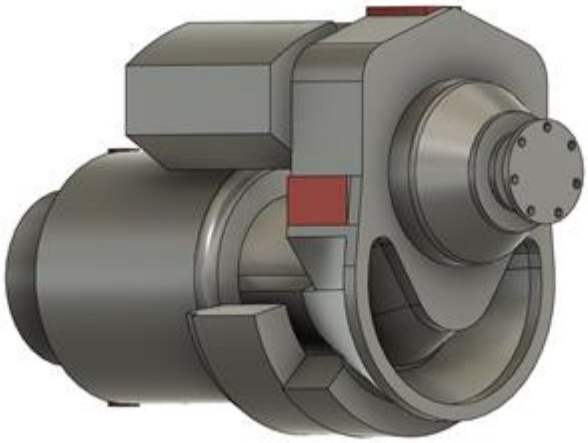

Figure 12. Model of TPE 331. Areas shown in red represent the frame mounting locations.

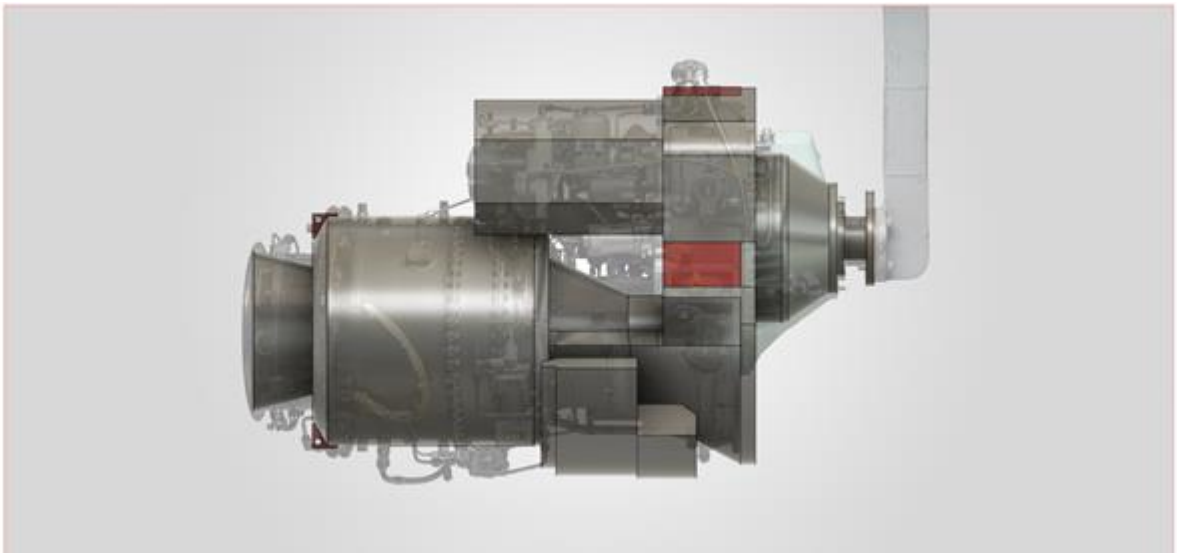

Figure 13. Model of TPE331 with background reference image.

F. Propellor Design

The propellor for this proposed aircraft has been designed to maximize efficiency to decrease operational costs and extend flight time to more easily accomplish requirements. This was accomplished using the OpenVSP modeling software and VSPAERO extension to design an analyze the design, respectively. This process resulted in a propellor with a 64.9-inch diameter, the maximum size to prevent interference with the ground during takeoff and landing and avoid the range of the combative hardware. The hub of the propellor is designed to lock directly to the shaft of the turbo-prop engine supplying power to the aircraft.

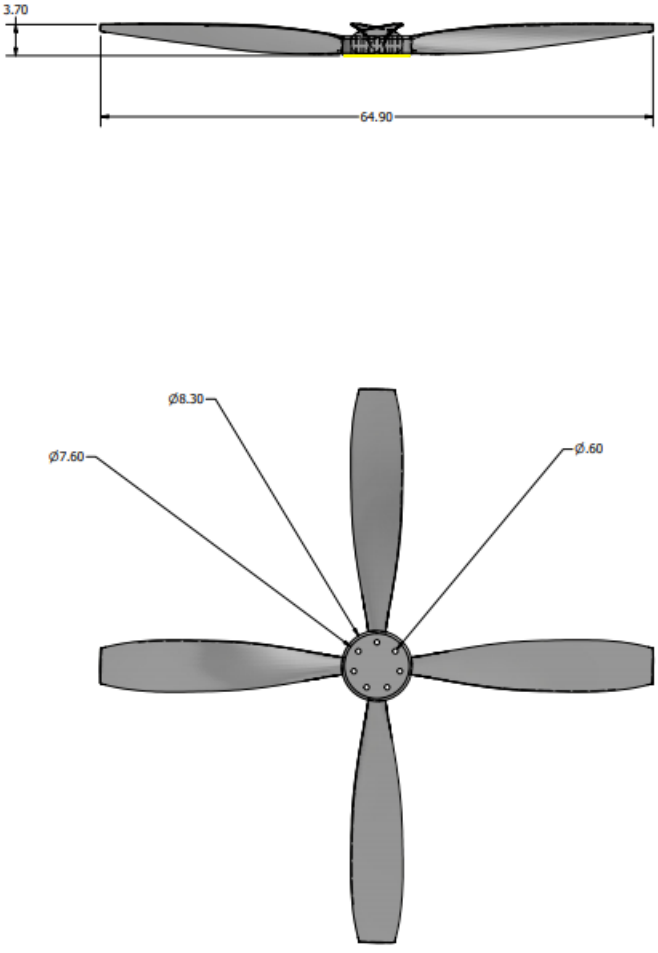

Figure 14. Propeller Dimensional Design

References

[1] https://www.aiaa.org/docs/default-source/uploadedfiles/education-and-careers/university-students/design-competitions/undergraduate-team-aircraft-design-competition/aiaa-2021-undergraduate-team-aircraft-design-rfp---light-attack-aircraft-2-.pdf?sfvrsn=b54e3cac_2

[2] https://www.globalsecurity.org/military/systems/aircraft/a-x-1966-design.htm

[3] https://www.grc.nasa.gov/www/k-12/airplane/aturbf.html

[4] https://www.faa.gov/regulations_policies/handbooks_manuals/aviation/airplane_handbook/media/17_afh_ch15.pdf

[5] https://airplaneacademy.com/piston-vs-turboprop-performance-efficiency-and-safety/

[6] https://www.faa.gov/regulations_policies/handbooks_manuals/aviation/airplane_handbook/media/16_afh_ch14.pdf

[7] https://www.pwc.ca/en/products-and-services/products/general-aviation-engines/pt6a

[8] https://aviationweek.com/business-aviation/used-aircraft-report-beech-king-air-b100

[9] https://aerospace.honeywell.com/content/dam/aero/en-us/documents/learn/products/engines/brochures/N61-1491-000-000-TPE331-10TurbopropEngine-bro.pdf

[9] https://aerospace.honeywell.com/content/dam/aero/en-us/documents/learn/products/engines/infographics/A40-1868-000-001-TPE331TurbopropEngine-ig.pdf

[10] https://aerospace.honeywell.com/en/learn/products/engines/tpe331-turboprop-engine

[11] https://martin-baker.com/products/mk12-ejection-seat/

[A] Sivakumar Ramakrishnan (2021). V-n Diagram (https://www.mathworks.com/matlabcentral/fileexchange/81793-v-n-diagram), MATLAB Central File Exchange. Retrieved May 15, 2021.

[B] Niu Ch‘un-yün. (1993). *Airframe structural design: March 22-26, 1993, Engineering 839.56: lecture notes*. University of California, Los Angeles, University Extension, Dept. of Engineering, Information Systems, and Technical Management, Short Course Program.

[#] *AT-6 Wolverine*. AT-6. (n.d.). https://defense.txtav.com/en/at-6.

[#] Portal Embraer. (n.d.). https://defense.embraer.com/global/en/super-tucano.

2021-2023 Composites Manufacturing Autoclave Design

This is a project that was started by myself and a small team of engineers at Texas Tech University operating withing the Raider Aerospace Society with the ambition of developing infrastructure to allow for greater capabilities for the range of design teams within the engineering college. We developed a design for an autoclave which has now been build and is being calibrated by engineers at the university continuing the project after my graduation. I served the project as a structural/thermal engineer and analyst for the pressure vessel, as well as designing the controls systems for the autoclave inlet which moderated the pressure and temperature of the autoclaves interior.

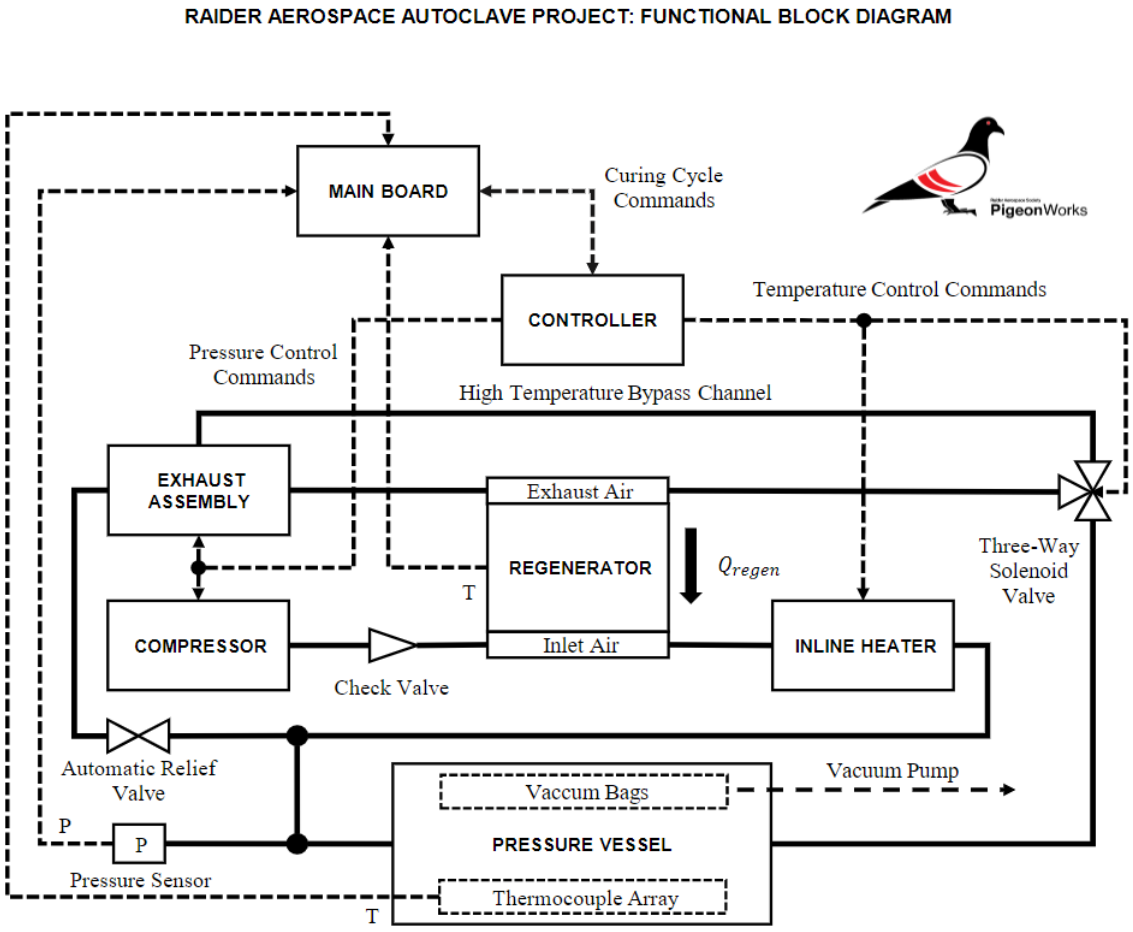

The above functional block diagram was developed by myself and the project manager to describe the flow of air, and the flow of sensory and command information between various components and the controller.

The following two images are taken from a presentation I did showing the steps taken to develop a structural analysis on the welded pipe section we used as a pressure vessel for the design. Much of the design for this section was developed by using industry standard components and manufacturing which allowed us to take advantage of pressure vessel certification without requiring successive failure tests. This allowed us to cut material, manufacturing, and testing costs substantially and spend more of our budget on controls systems. These systems could then allow for higher fidelity in our composite manufacturing cycles and improve part quality once in operation. We did however want to ensure we did our own analysis of the structure, so I verified the system with hand calculations and with an FEA model.

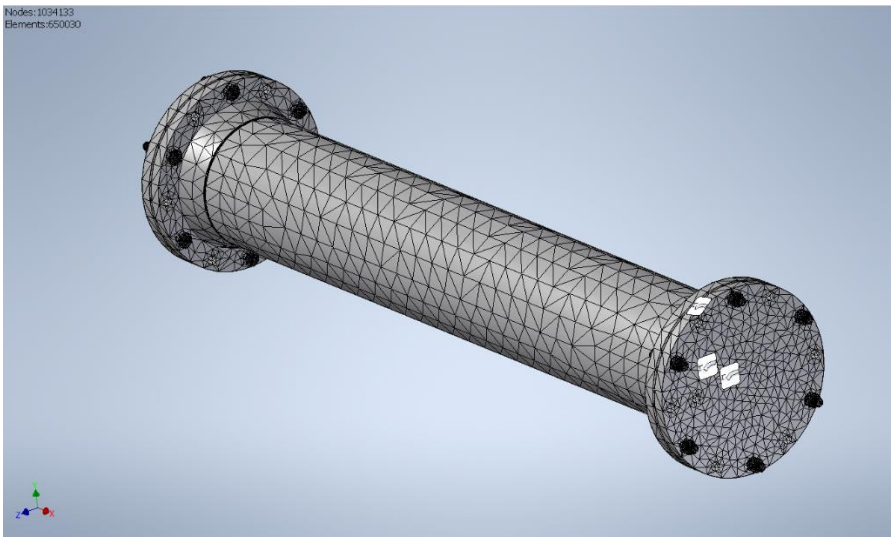

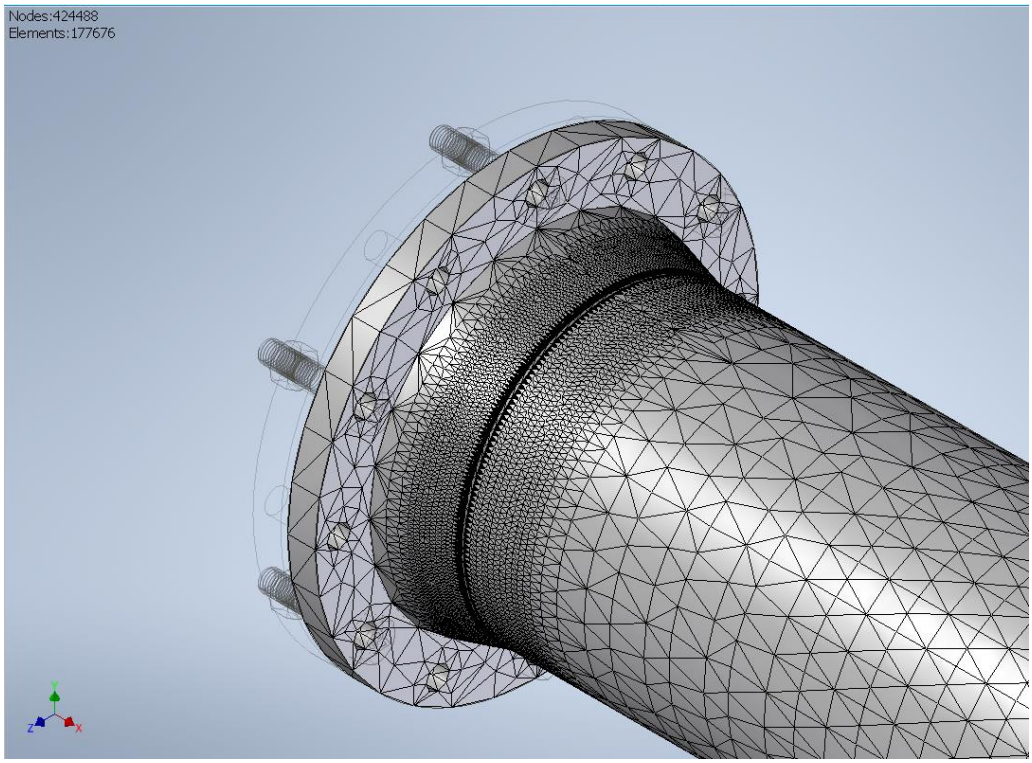

A mesh refinement was performed on the weld joint to ensure the weak point in the system was properly analyzed. This location in the design is also a geometric discontinuity so in addition to the induced stresses from welding this is a location of concern for the pressure vessel.

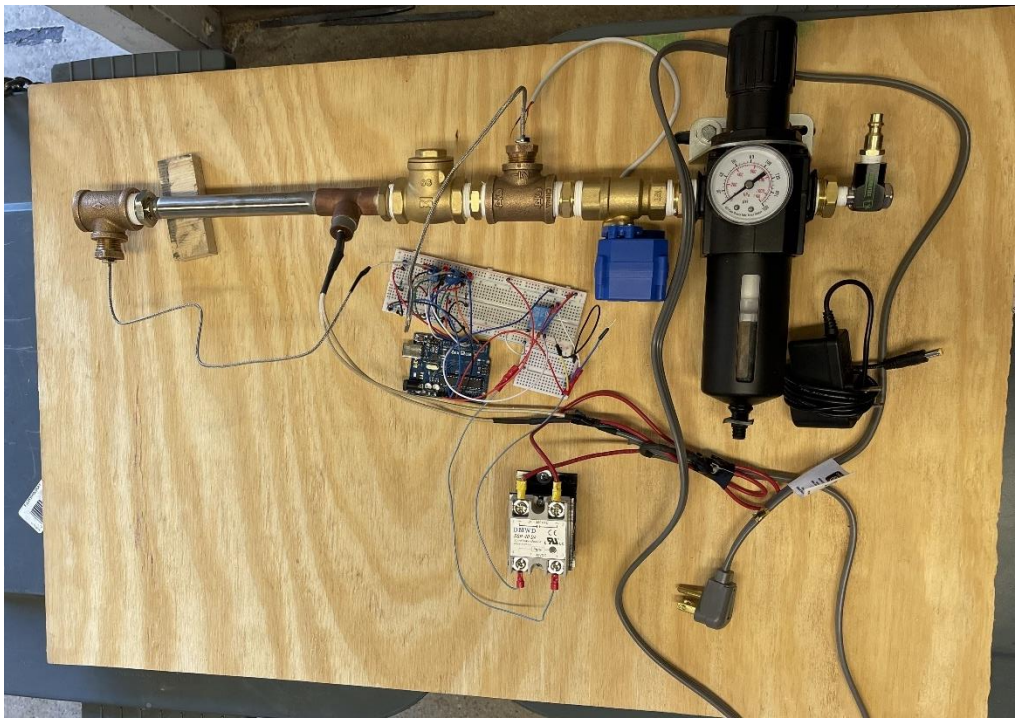

I build the autoclave inlet system and the electronic circuitry to deliver power to heating elements and valves, as well as process pressure and temperature data to make modifications to operating conditions.

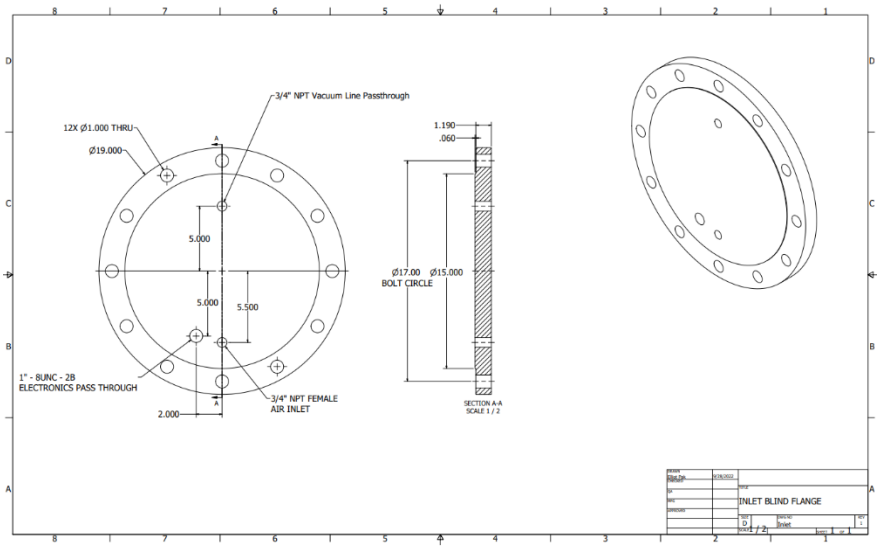

The end caps for the pressure vessel were designed as modifications to blind flanges the can be purchased off the market. The inlet side end cap was designed to have three holes drilled into them to allow for electronics and air to enter and exit the chamber. These would allow for air to be evacuated from the parts, the chamber to be pressurized and heated, and for probes necessary to collecting data to be inserted without compromising the seal.

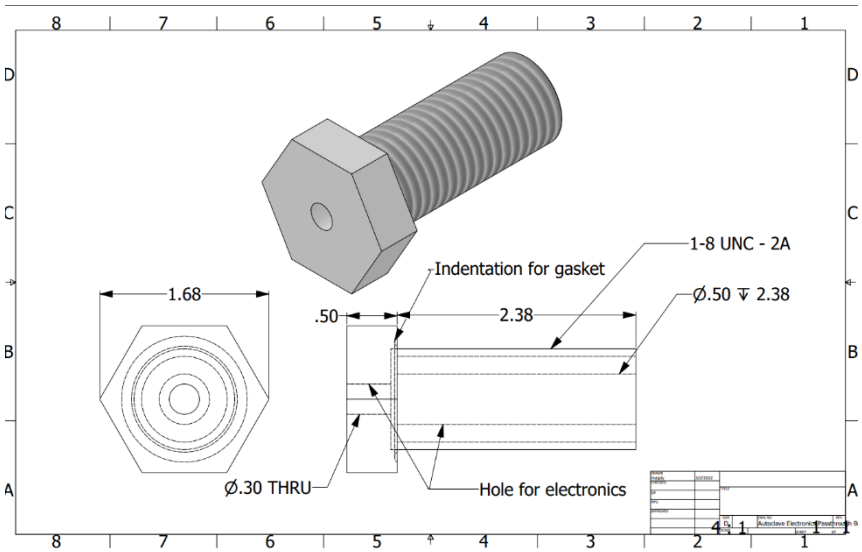

For the electronics passthrough a specialized bolt was designed to be able to pass the electronic wiring though, then be epoxied in with a temperature and pressure safe epoxy.

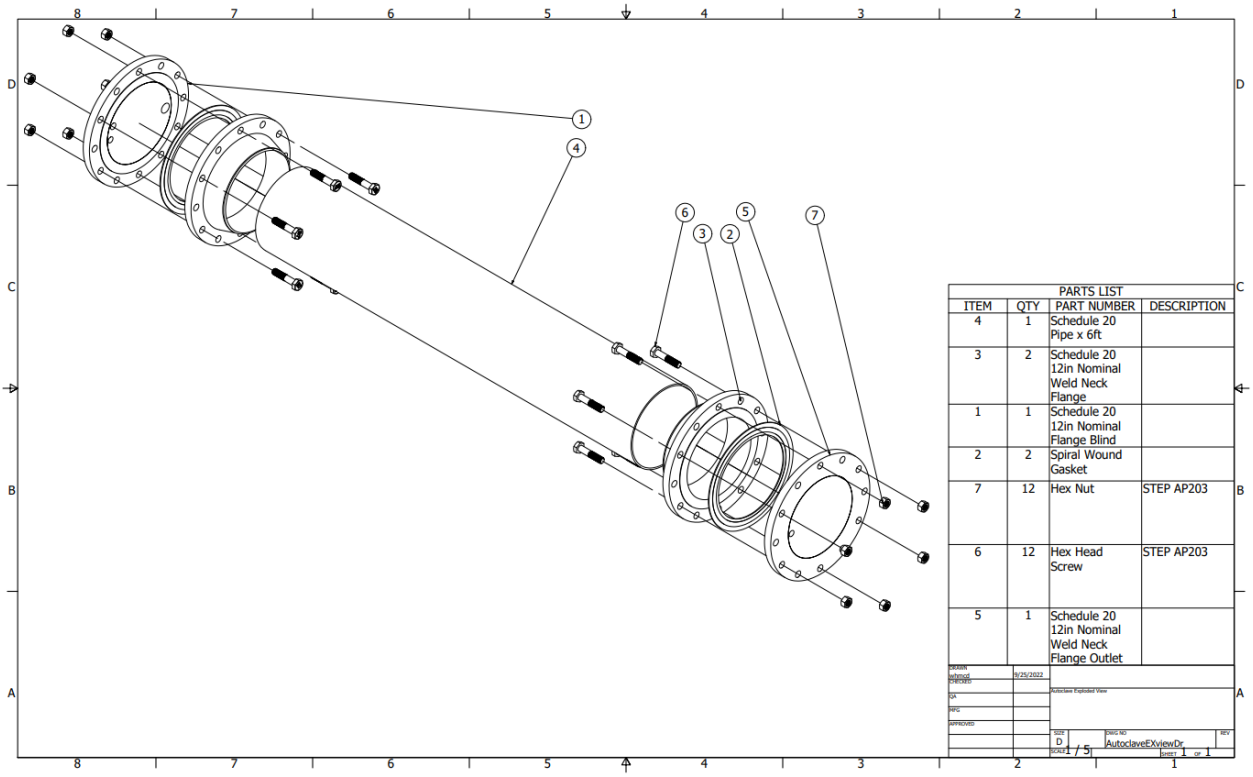

Exploded View of Pressure Vessel Assembly

NASA VTOL Air Taxi – TTU Aerodynamics and Flow Control Lab

In the course of working on the Urban Transportation Air Taxi project in the Aerodynamics Lab, I worked with the wind tunnel team on developing a model which can be used in manufacturing.

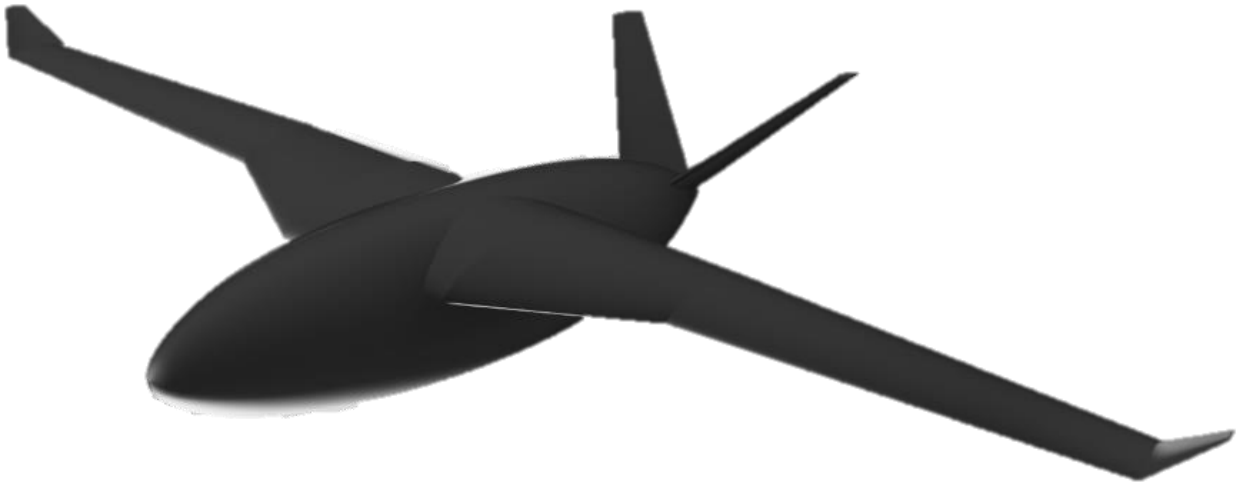

Fig. 1 – Full Inventor Model of Air Taxi

Figure 1 shows the model I developed using the aircraft geometry given to me as a .vsp file. This geometry was then used in the creating of parts to by additively manufactured and finished with internal hexagonal structure which is necessary for the strength and stability of the model under strong aerodynamic loads.

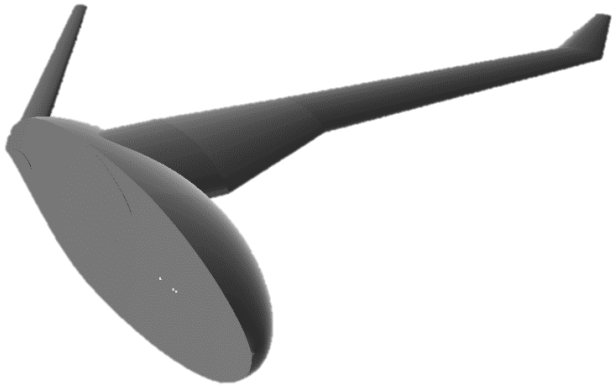

Fig. 2 – Half Section at Wind Tunnel Scale

Once I had successfully created this model, I created a symmetrical half section of the aircraft shown in Figure 2 to be used in making of a wind tunnel section in ANSYS for analysis.

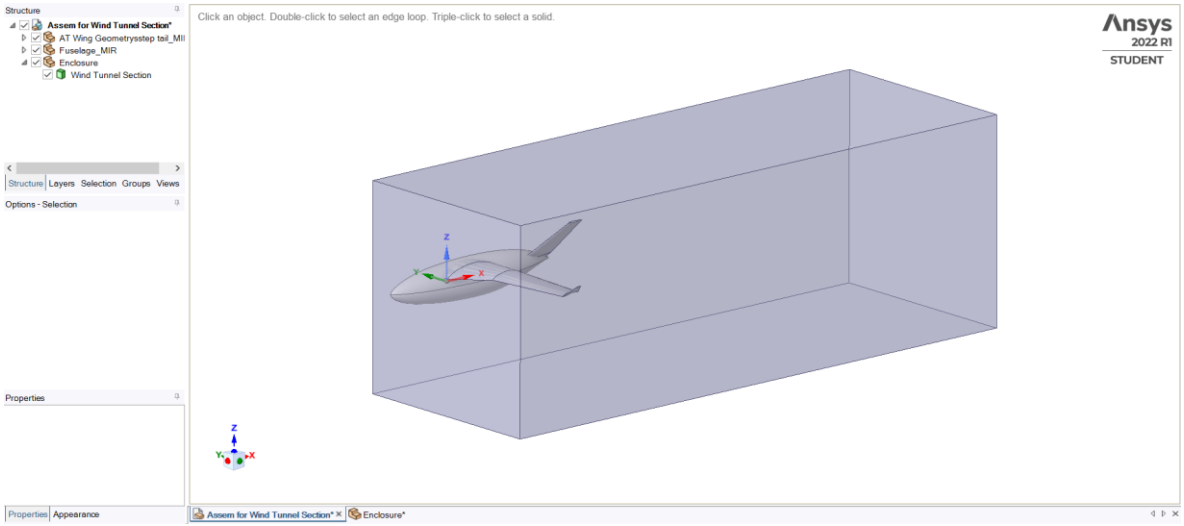

Fig. 3 – ANSYS SpaceClaim Geometry of Wind Tunnel Section

Figure 3 displays the wind tunnel geometry I developed for the purposes of computational simulation for this aircraft. The model is set up to allow for the simulation of downstream affects in the flow. This will allow for the development of and calibration of an accurate flow model which can be used in extended case modelling outside of what is possible in the university's facilities, as well as a more comprehensive fluid flow model that can help in further design iterations.

The following is the full paper of which I was part of writing for full project context. In addition to working with the team on the paper's development, I contributed to sections C and G of this paper where I described the operation of current turbine technology and that of the concept. In addition, I descried the major challenges which face this type of design given the mechanics of jet propulsion.

Conceptual Design of a Single Core Mixed Pressure Flow Hybrid Electric Turbine Engine

Nazir Gandur*, Guilherme D. Fernandes†, Jeremy Wilkey, Anthony Valencia, Nolan T. Shelton, Adrian Brink, Santos Ramirez, Patel S.K. and Victor Hugo Maldonado‡
Texas Tech University, Lubbock, TX, 79409

The next generation of commercial regional transports are envisioned to use hybrid electric propulsion to reduce CO_2 emissions and noise, while maintaining the cruise speed and range required to be practical for shorter regional routes. This paper explores the design of a single-core, mixed pressure flow hybrid electric turbine engine to bridge the gap between current fossil fueled turbofan engines and fully electric propulsion. Our main objective was to evaluate the pressure increase in an open-flow setting by the use of counter-rotating rotors driven by electric motors. The pressure gradient in the radial direction must be minimized, keeping the flow attached to the outer portion of the rotor blades. Our design features variable sweep blades in order to make this possible. Unlike regular turbine engines, our design features a simpler mechanical build which uses electric motors, rather than a shaft driven by a turbine, to drive the fan and the counter-rotating compressor stages. The compression rate and possibility of flow separation over the compressor blades are studied by the use of Computational Fluid Dynamics (CFD) to determine whether the design is feasible. Our results show that it is possible to attain pressure increase in the inner portion while keeping the flow mostly attached, although further research is necessary on the concept.

I. Introduction

The aviation industry is under pressure to reduce carbon emissions while meeting rising demand for air travel. This research paper investigates the feasibility of the Hybrid Electric Turbine Engine (HETE), a promising technology that combines gas turbine efficiency with the environmental benefits of electric propulsion [1]. The paper investigates the HETE's design and operational features, as well as the findings of a survey on the current state of electric vehicles in the field. Overall, the paper emphasizes the importance of HETE as a potential solution for reducing emissions in the aviation industry, as well as providing insights into the most recent developments in electric turbine engine technology.

A. State of the Art

In terms of cutting edge technology for regular turbine engines, General electric produces the GE9X turbine [2], which is used in the family of Boeing 777X's. The GE9X engine is special in the sense that it is currently the most efficient, and one of the most powerful turbofans in production. This is achieved by using additive manufacturing, usually with titanium filament, to achieve significant weight reductions for the compressor section and fan sections of the turbine. Additive manufacturing has not only allowed for significant increases in efficiency and power, but also reduction of noise levels as well.

The research development of hybrid aircraft [3] and hybrid propulsion systems design and energy management is a subject of opportunity for the development of hybrid engines. In the context of relatively underdeveloped electrical storage technologies, the study of mid-scale hybrid aircraft can contribute the most to theoretical and practical knowledge. Meanwhile, the benefits and drawbacks of using hybrid propulsion in mid-size hybrid aircraft have not been thoroughly demonstrated [4, 5], as well as its potential advantages and challenges for the aviation industry. Perhaps one future possible applications for a hybrid engine is in the USAF's NGAS program, which emphasizes fuel economy [6].

Currently, research on the conceptual design of hybrid aircraft using multi-objective optimization is lacking. Furthermore, there is a research gap in the consideration of aircraft safety in current hybrid ground vehicle methodologies. Furthermore, for complex flight missions with multiple sub-tasks, both non-causal and causal energy management

[*]Ph.D. Candidate, Mechanical Engineering, Texas Tech University, Box 41021 | Lubbock, TX 79409

[†]Ph.D. Candidate, Mechanical Engineering, Texas Tech University, Box 41021 | Lubbock, TX 79409

[‡]Associate Professor, Mechanical Engineering, Texas Tech University, Box 41021 | Lubbock, TX 79409

strategies are required. Overall, these findings highlight the need for additional research and development in the design and energy management of hybrid aircraft, with a focus on multi-objective optimization and aircraft safety considerations.

B. Environmental Considerations

According to United Nations (UN) guidelines, global greenhouse gas emissions must peak before 2025 and then decline by 43 percent by 2030 and to net zero by 2050. Extensive review on greenhouse emissions by transport type [7] reveals that aviation accounts for only 13.3% of emissions; however, the aviation industry has been focusing more on electric and hybrid propulsion, especially for regional transportation, with the most notable example perhaps being the Lilium jet.

Despite a major global effort, battery technology is still the limiting factor for fully electric propulsion. The major manufacturers of turbine engines are also focused on increasing the efficiency of existing turbine engines. Moreover, the extensive use of composite materials in aviation has lowered the thrust demand, further contributing to lower emissions. Contributions in both fields will have a direct application towards the HETE project and future fully electric engines.

C. Current turbine technology and the HETE concept

To fully grasp the concept of the hybrid electric-turbine engine, we must first explain how a conventional turbine engine operates. A turbine engine and its working fluid are similar to a normal piston cylinder engine, where air and fuel are combined to produce work. Turbines operate by taking air into the air inlet and then continuing towards guide vanes that modulate the air by opening and closing the blades to increase or reduce the mass-flow rate throughout the operation of the turbine. Once the air passes through the guide vanes, the air then travels to the compressor stages, with both stationary and rotating blades, where air is compressed and heated. After this stage, air is sent to the combustion chamber and then ignited with the proper air fuel mixture using nozzles. To increase turbine efficiency, part of the air is sent through a bypass [8]. An overview of current turbine technology is available in [9].

A modern turbofan engine operates accelerating ambient air with a fan and then bypassing some low-pressure air through an outer stage around the inner high-pressure compressor, burner, and turbine to achieve a greater efficiency than a traditional turbojet engine is capable of achieving. The air bypassed around the inner stage of the engine flows at a higher velocity than the ambient and therefore produces thrust along with the high-pressure inner stage when they both expanded through a jet nozzle. In traditional designs, the ducted fan or initial low-pressure compressor is driven off the turbine in the interior stage. An important metric for determining the efficiency of a turbofan engine is the bypass ratio, the ratio of bypass flow to interior flow rate, having significant impacts on thrust per air flow rate and thrust specific fuel consumption. A major compromise in a traditional turbofan design is that the separation of the two flows is achieved with a casing which increases weight and overall engine size, contributing to higher lift requirements and nacelle drag [6, 10–12].

To explain how the HETE engine functions, it is important to understand the differences between an electric motor and a traditional turbine engine. There are a few important advantages to an electric motor that we intend to capitalize on, the first being efficiency. Modern electric motors achieve a 90% or higher efficiency in converting electric power to mechanical power to drive a rotor or propeller. The next is reduced noise; electric motors are significantly quieter than turbine engines, which is especially important when operating in urban areas. As far as maintenance costs are concerned, compared to the electric motor, turbine engines have more moving parts that are also more complex, increasing the likelihood of mechanical failure [13–15] and thus performing more regular maintenance. The complex critical systems of aircraft electric motors necessitate a model-based framework capable of managing variability and uncertainty [16–19], encompassing factors such as sensor noise and modeling imperfections. Manufacturers increasingly embrace digital twins [20, 21] to simulate entire engine fleets and monitor their operations. This data-driven approach, implemented on digital platforms, optimizes both flight operations and maintenance processes, resulting in consistent cost savings for airlines. The current drawbacks of electric motors are the limited range and weight of the aircraft, since electric motors and batteries especially are significantly heavier than turbine engines, and with a lower energy density than fossil fuels. Couple that with the fact that batteries degrade at a higher rate and that the infrastructure is not currently in place to support the charging of the batteries, and electric motors become less feasible for long-range flights.

One example of short range flight is the Eviation Alice, an aircraft using two electric motors. Designed to accommodate nine passengers in addition to its two crew members, the plane flew its inaugural flight on September 27, 2022, when it flew for eight minutes. This seems like a small achievement, however considering that propulsion technology has not changed in years, it is a monumental feat that proves the viability of electric motors. Eviation's

president and CEO, Gregory Davis, said as much in an interview with CNN, “We have not seen the propulsion technology change on the aircraft since we went from the piston engine to the turbine engine. It was the 1950s that was the last time you saw an entirely new technology like this come together.” The intended capabilities of Alice are a max takeoff weight of 18,400 lbs with a max total payload of 5,100 lbs and a range of 290 miles and a max speed of 300 mph. With recharging stations located at each landing site, a plane of these capabilities would excel in making short passenger transport flights from city to city with no emissions and low cost for energy.

Technology still has a long way to mature before electric aircraft are capable of making long-distance flights. As such, our evaluation is that current electric propulsion alternatives are best used in conjunction with a traditional turbine engine. This is where the HETE comes into play, combining both the reliability of the turbine engine with the efficiency and reduced emissions of the electric motor.

The HETE engine combines the thrust and operating time of a turbofan engine with the efficiency and lower noise use of an electric motor system. Electric motors can also function as generators during descent, harvesting energy that can be stored in batteries and reduce the charging time required for the next flight. This study will investigate the HETE’s key design elements and operational characteristics, as well as its potential benefits and problems for the aviation sector.

D. Design and Operation

The HETE concept is comprised of a frontal fan and a number of counter-rotating stages, each referred to as a "compression unit" and annular combustors. An overview of the design can be seen in Fig. 1. Flow enters through the fan, shown in green, and is directed to the compressor stages, shown in yellow. Each compressor stage consists of a pair of contra-rotating rotors driven by electrical motors. Unlike traditional turbofan engines, in the HETE there is no physical partition between the compression region and the bypass region, characterizing the unique mixed flow features of the project. A portion of the fluid that undergoes combustion, in the red annular combustors. The rate of combustion can be ajusted so that the "inner" flow region provides the majority of the power during takeoff and climb, the two portions of the mission requiring the most power. The entire design can be optimized in such a way to minimize the usage of fossile fuel during cruise, when electric fan supplies the majority of power. At the current state of this concept, we assume that the angular velocity of each rotor can be controlled in such a way that variable inlet guide vanes are not necessary.

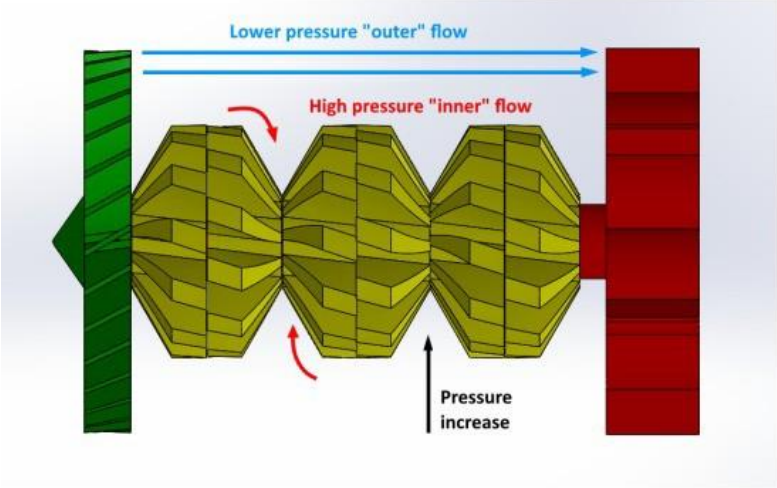

Fig. 1 Side view schematic of the HETE design.

It is difficult to define such thing as a bypass ratio for a mixed flow engine, but the HETE can be seen as a variable bypass hybrid engine. Another difference from regular turbofans is the absence of the turbine after the combustor. Since we opted to use electric motors do drive the fan and the compression stages, there is no need to further extract energy from the fluid to drive those components through a shaft. One immediate advantage of that choice is that the back work ratio is zero, and therefore all of the flow energy can be used to generate thrust; therefore, it is not necessary to elevate the enthalpy as much as in regular turbofans. This makes it possible for the HETE to operate at lower overall pressure ratios.

Perhaps the biggest challenge of the HETE design is the pressure gradient in the radial direction. Since there is no confinement for the portion of the flow going through compression, there is a tendency of outward movement, causing pressure loss and mixing with the outer region. In theory, this could be used to enhance mixing of the fuel-air mixture, but the most significant effect is less efficient compression, resulting in a lower pressure ratio. In our design, this problem is tackled by two different avenues. The first one is a choice of a lower pressure ratio, of about 5:1 as explained previously; the second is the special design of the compressor blades, where variable twist is applied in order to keep the flow attached to the blades.

A view of the first pair of contra-rotating rotors, which comprise the first compressor stage, can be seen in Fig. 2. The blade is designed so that the inner portion resembles a compressor blade and the outer portion resembles an actual propeller. By applying a smooth transition, the pressure gradient in the radial direction can be minimized. Here, it makes no sense to name the two propellers as "rotor" and "stator". The angles of attack for the inner portions of each rotor are chosen to match the classic configuration for axial compressors. The angles of attack for the outer portions of each blade are chosen to match the configuration of contra-rotating turboprop aircraft such as the Russian Tu-95 bomber.

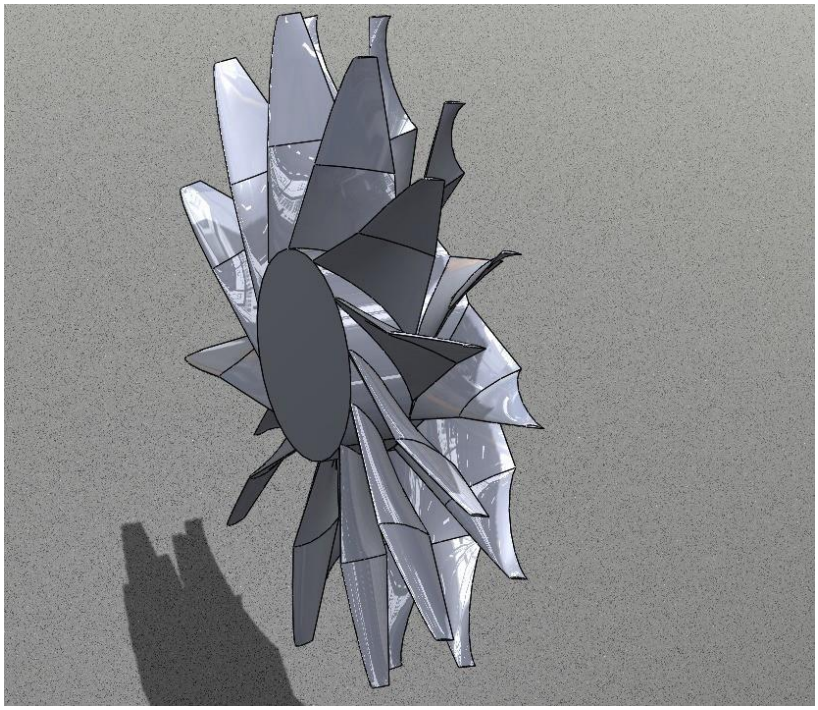

Fig. 2 Rotor design with high pressure blade root and low pressure blade tip.

The feasibility of the design will be investigated through the use of CFD to determine if the design challenges can be overcame by proper dimension choices for the propeller and compressor blades, as well adequate choices for the rotating velocities for each electric motor. The design of the blades for each pair of rotors has to be unique in order to produce maximum compression while keeping the flow attached to the blade, just like in axial compressors. Expected results include velocity and pressure data for all points inside of the engine, as well as visualization of the trailing vortices for the compressor stages, which will answer the two questions of the current paper.

E. Advantages

One of the most significant advantages of the HETE is its ability to minimize fuel usage and pollutants. The HETE could dramatically lower the aviation industry's carbon footprint by combining the efficiency of a gas turbine engine with the environmental benefits of electric power. The use of an electric motor in the hybrid system can significantly reduce emissions and improve air quality, making it a more environmentally friendly option. The point of operation can be adjusted to deliver additional power output when needed, which can be particularly useful in certain portions of the flight such as takeoff and hover. However, this flexibility also makes it an option for applications other than regional aviation, such as long haul aircraft and military vehicles. The hybrid system can provide greater flexibility in power

management, as the electric motor can be used for auxiliary power, energy recovery, and regenerative braking. Similarly, the use of multiple power sources can increase the overall reliability of the hybrid system, as there is redundancy in case of an engine failure. Continuously, the electric component of the hybrid system allows for energy storage, which can reduce dependence on fossil fuels and provide backup power in case of an emergency. Additionally, the electric component of the hybrid system allows for silent operation, which can be beneficial in certain applications, such as aircraft and drones. This is advantageous because the hybrid system can also maintain power output at high altitudes, where gas turbines may struggle due to reduced air density. Lastly, the hybrid system can reduce maintenance costs over time, as the electric motor can operate without the need for regular maintenance, unlike current gas turbines.

F. Disadvantages

Despite its potential benefits, the HETE confronts a number of hurdles. The weight of the electric motor/generator system and battery storage system, which might add significant weight to the aircraft and restrict its payload capacity, is one of the key problems. Furthermore, the HETE necessitates considerable adjustments to the aircraft's architecture and electrical systems, which may be expensive and time-consuming. Additionally, the availability of charging infrastructure can be a limiting factor for the adoption of hybrid electric turbine engines, particularly in remote areas. For instance, the range of a hybrid electric turbine engine can be limited by the capacity of the battery, which can impact the viability of the system for certain applications, such as long-haul flights. Moreover, the power output of the electric motor may be limited by the size and capacity of the battery, which can further limit the potential of the system. On the other hand, the use of batteries in the hybrid system can pose safety risks, particularly in applications where there is a high risk of impact or fire. Therefore, the regulations governing hybrid electric turbine engines may be more complex than those for conventional gas turbine engines, which can limit their adoption in certain industries. All in all, it is important to note that the technology for hybrid electric turbine engines is still in the early stages of development, and there may be significant challenges in scaling up and commercializing the technology.

G. Design Hurdles

The primary design hurdle is in the characterization of the boundary conditions between the low pressure "outer flow" and high pressure "inner flow" and determining favorable effective bypass. This is challenging to simulate in software and has a significant impact on the potential efficiency of the proposed design. In addition, tip vortices have an even bigger impact in the absence of a mechanical boundary around the compressor stages air they can disrupt the airflow of the bypass air, causing a significant power loss. Tip vortices can cause disruptions in airflow in the engine, which can yield compressor stalls and engine flame-outs. To overcome the challenges of software simulation limitations, each blade was design and tested to ensure the pressure stayed attached to the blades as intended in the design stages. To counteract this vortex phenomenon, the fan and compressor rotors have been designed with a gradient reduction from the center of the rotor to the rotor tip in order to keep the flow attached to the blades. This design led to the creation a triangular geometry that yields pressure generation towards the center of the rotors, mitigating the production of tip vortices. The reduction of tip vortices assists in the separation of the high pressure of the inner flows from the low pressure of the outer flows, creating a boundary layer to allow the bypass air to efficiently flow to the combustion chamber.

II. Simulation

The first pair of rotors that forms the compressor stage was modeled in Solidworks (Fig.2). The hub diameter is 0.4 m and the blade diameter is 1.2 m. Both rotors have 12 blades, and their profiles feature NACA 6000 series airfoils. Since we are investigating a small portion of what is still a preliminary concept, we chose to use a vortex panel method solver (Flightstream), which is accurate enough for rotors and ducted fans. The unsteady solver is set up so that the blade undergoes 9° of rotation in each time step. The number of time steps is chosen such that each rotor completes two full revolutions.

For better accuracy, viscous coupling was enabled and separation features were turned on, utilizing an axial separation model. The angular velocity for each rotor is 1200 RPM. Vortex panel methods require a surface mesh instead of a volume mesh. In particular, the simulation is set up utilizing only one blade and taking advantage of circular symmetry for both rotors and the outer casing. This allows for significant time savings when compared to classic CFD software such as ANSYS Fluent. The mesh is shown in Fig. 3. The inflow velocity is 100 m/s.

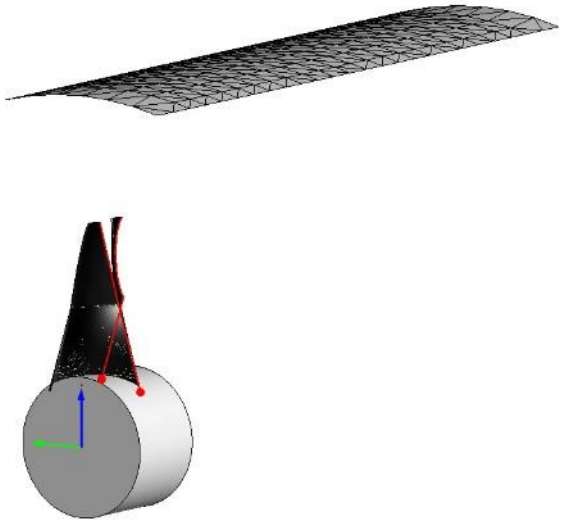

Fig. 3 Mesh for the basic compression unit. In order to save computational time, we made use of circular symmetry by repeating the pattern 12 times.

III. Preliminary Results

Figure 4 shows the coefficient of pressure at each point for the first two blades. The streamlines are shown in Fig. 5. The flow stays attached to the blades. The pressure increase for the first stage is 20% for the inner portion of flow.

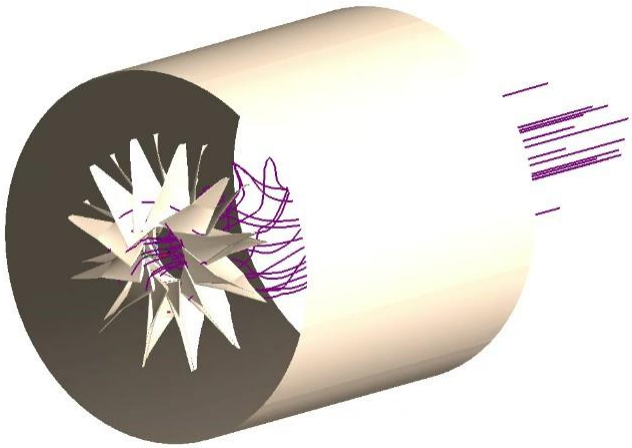

Fig. 4 Coefficient of pressure for the first two counter rotating propellers.

IV. Conclusion

After performing simulation in ANSYS to evaluate the pressure increase in an open-flow setting by the use of counter-rotating propellers driven by electric motors, some conclusions can be drawn. First, the simulation can provide information on the pressure gradient in the radial direction of the compressor blades. By minimizing this pressure

gradient, the blades can be designed to keep the flow attached to the outer portion of the blades, which can improve the efficiency and reliability of the compressor stages. Second, the simulation can provide information on the performance of the counter-rotating rotors and the electric motors driving them. This information can be used to optimize the design of the rotors and motors for maximum efficiency and power output.

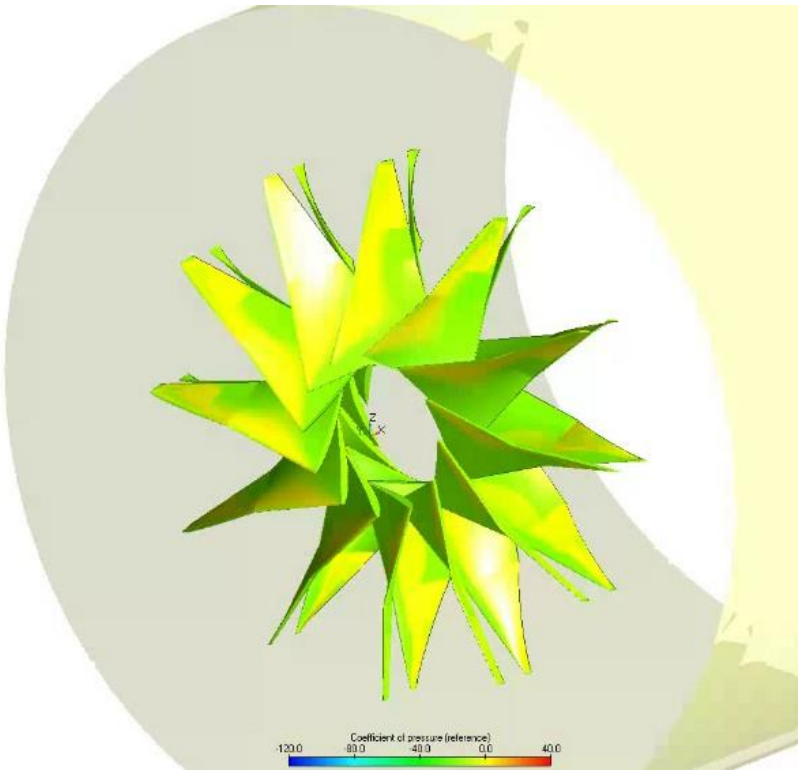

Fig. 5 Streamlines generated by the first pair of counter rotating rotors.

Finally, the simulation can provide information on the overall performance of the compressor in terms of pressure increase and power consumption. This information can be used to evaluate the effectiveness of the compressor and identify any areas for improvement in its design or operation. Overall, a rotor simulation in ANSYS can provide valuable insights into the performance of a compressor in an open-flow setting with counter-rotating rotors driven by electric motors. By optimizing the design of the compressor and its components, our team will improve its efficiency and reliability, which can have significant benefits in various applications such as in aircraft engines or in gas compression for industrial purposes.

References

[1] Burke, A., "Hybrid/Electric Vehicle Design Options and Evaluations," *SAE Technical Paper*, 1992. https://doi.org/10.4271/920447.

[2] Granovskii, M., Dincer, I., and Rosen, M. A., "Economic and environmental comparison of conventional, hybrid, electric and hydrogen fuel cell vehicles," *Journal of Power Sources*, Vol. 159, No. 2, 2006, pp. 1186–1193. https://doi.org/https://doi.org/10.1016/j.jpowsour.2005.11.086, URL https://www.sciencedirect.com/science/article/pii/S0378775305016502.

[3] Rosario, R. d., "A future with hybrid electric propulsion systems: A NASA perspective - NASA technical reports server (NTRS)," , ???? URL https://ntrs.nasa.gov/citations/20150000748.

[4] Pornet, C., and Isikveren, A., "Conceptual design of hybrid-electric transport aircraft," *Progress in Aerospace Sciences*, Vol. 79, 2015, pp. 114–135. https://doi.org/https://doi.org/10.1016/j.paerosci.2015.09.002, URL https://www.sciencedirect.com/science/article/pii/S0376042115300130.

[5] Gesell, H., Wolters, F., and Plohr, M., "System analysis of turbo-electric and hybrid-electric propulsion systems on a regional aircraft," *The Aeronautical Journal*, Vol. 123, No. 1268, 2019, p. 1602–1617. https://doi.org/10.1017/aer.2019.61.

[6] Guilherme D. Fernandes, A. M. J. P. D. K. C. M. V. E. H. K. D. M. E. R., Nazir Laureano Gandur, and Maldonado, V., "Conceptual Design of a Semi Blended Wing Body for the Air Force Next-Generation Air-Refueling system," *AIAA SciTech 2024*, American Institute of Aeronautics and Astronautics (AIAA), Orlando, Florida, 2024. Accepted.

[7] Fan, Y. V., Perry, S., Klemeš, J. J., and Lee, C. T., "A review on air emissions assessment: Transportation," *Journal of Cleaner Production*, Vol. 194, 2018, pp. 673–684. https://doi.org/10.1016/j.jclepro.2018.05.151, URL https://doi.org/10.1016/j.jclepro.
2018.05.151.

[8] Gandur, N. L., *A Matemática e a Física do CP-CEM, 2nd edition*, Vestseller, Brazil, 2023. Book.

[9] Mattingly, J. D., Heiser, W. H., and Pratt, D. T., *Aircraft Engine Design, Second Edition*, American Institute of Aeronautics and Astronautics, 2002. https://doi.org/10.2514/4.861444, URL https://doi.org/10.2514/4.861444.

[10] Fernandes, G., Gandur, N. L., Santos, D., and Maldonado, V., "The sub 2-hour official marathon is possible: developing a drafting strategy for a historic breakthrough in sports," 2023. https://doi.org/10.21203/rs.3.rs-3390553/v1, URL http:
//dx.doi.org/10.21203/rs.3.rs-3390553/v1.

[11] Fernandes, G. D., and Maldonado, V., "The Sub 2-Hour Marathon Is at Hand: How Kelvin Kiptum Can Use Drafting to Improve His Impressive World Record," 2023. https://doi.org/10.20944/preprints202310.1598.v1, URL http://dx.doi.org/10. 20944/preprints202310.1598.v1.

[12] Fernandes, G., and Maldonado, V., "Against negative splitting: the case for alternative pacing strategies for elite marathon athletes in official events," , 2023. https://doi.org/10.48550/ARXIV.2311.08645, URL https://arxiv.org/abs/2311.08645.

[13] Ekwaro-Osire, S., Gandur, N. L., and Lopez-Salazar, C. A., "Incipient Fault Point Detection Based on Multiscale Diversity Entropy," *Journal of Nondestructive Evaluation, Diagnostics and Prognostics of Engineering Systems*, Vol. 6, No. 3, 2023.

[14] da Rocha, G. B. T., Pereira, L. M. M., Farias, L. D. P., Gandur, N. L., Flores, P. M., and de Oliveira, R. M., "Análise fractográfica em MEV–fratura dúctil x fratura frágil," 2016.

[15] Gandur, N. L., and Osire, S. E., "Uncertainty Quantification in the Prediction of Remaining Useful Life Considering Multiple Failure Modes," *Proceedings of the ASME 2023 International Mechanical Engineering Congress and Exposition (IMECE2023)*, American Society of Mechanical Engineers (ASME), New Orleans, Louisiana, 2023.

[16] Yanik, Y., Da Silva, S., and Cunha Jr, A., "Uncertainty quantification in the comparison of structural criterions of failure," *X Congresso Nacional de Engenharia Mecânica (CONEM 2018)*, 2018.

[17] Yanik, Y., "Quantification of parametric uncertainties effects in structural failure criteria," 2019.

[18] Cunha, A., Yanik, Y., Olivieri, C., and da Silva, S., "Tresca vs. von Mises: Which failure criterion is more conservative in a probabilistic context?" *Journal of Applied Mechanics*, 2023, pp. 1–8.

[19] Fernandes, G., and Maldonado, V., "Behavioral aspects and the transmission of Monkeypox: A novel approach to determine the probability of transmission for sexually transmissible diseases," *Infectious Disease Modelling*, Vol. 8, No. 3, 2023, p. 842–854. https://doi.org/10.1016/j.idm.2023.07.008, URL http://dx.doi.org/10.1016/j.idm.2023.07.008.

[20] Yanik, Y., Ekwaro-Osire, S., Dias, J. P., Porto, E. H., Alves, D., Machado, T. H., Bregion Daniel, G., de Castro, H. F., and Cavalca, K. L., "Verification and Validation of Rotating Machinery Using Digital Twin," *ASCE-ASME J Risk and Uncert in Engrg Sys Part B Mech Engrg*, 2023, pp. 1–42.

Yüce, C., Gecgel, O., Doğan, O.,

Dabetwar, S., Yanik, Y., Kalay, O. C., Karpat, E., Karpat, F., and Ekwaro-Osire, S., "Prognostics and health management of wind energy infrastructure systems," *ASCE-ASME Journal of Risk and Uncertainty in*

The following report is a capstone project for a course over forensic engineering and Failure Analysis for which I performed a root cause failure analysis on the pump system which was determined to be the center of an industrial fire at a petro-chemical processing plant. I was supplied a collection of primary data in the form of images both from on site and from lab spectroscopy. However, the analysis of the evidence and discussion of conclusions is original to myself.

Incident Summary

This failure investigation will look into the root cause of an incident taking place in a petro-chemical refinery which resulted in a fire that ignited 15 storage tanks and a substantial quantity of petrochemical products and injury to workers in the direct area as well as exposure of the entire facility to harmful fumes. As a result, the refiner and the manufacturer of the pump and its components have been sued for damages to the employees affected.

Leading up to ignition there was a spill of petrochemical products from a pumping station which serviced storage tanks, allowing the 8500 gallons of spilled flammable product the opportunity to catch fire and for that fire to spread to nearby storage tanks which continued to burn for several days.

It is believed, from the investigation of fire spread and data from the operation of the facility leading up to the fire, that the seal of a pump at the pumping station at the center of the fire had detached from the pump and allowed the chemical to come free. This failed component was accompanied by a number of other failed components which attached to it including a galled shaft, worn and deformed ball bearings, loose bolts, and broken pump pedestals.

Discussion of Evidence

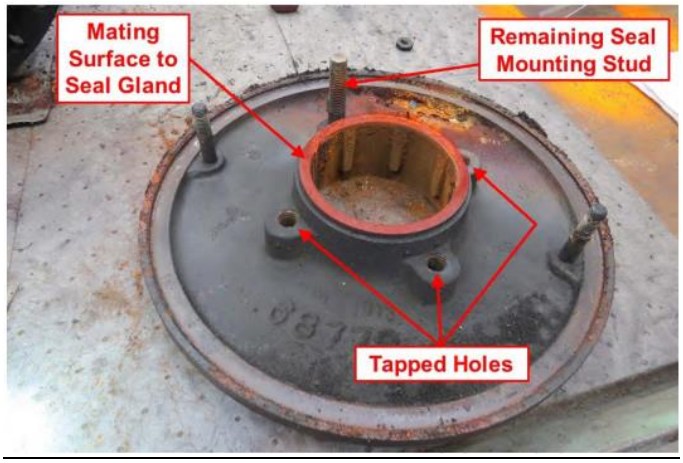

Fig. 1 – Seal Chamber Face Plate

The mating surface where the seal gland in figure 1 meets the seal chamber shows significant buildup of red characteristic rust which forms under high oxygen, high moisture conditions which are seen in other areas on various components as well. This type is not what you would expect to see from a fire accelerated oxidation of these components, of which you can see as yellow rust covering other sections of this part seen in Figure 1 and throughout the subject pump.

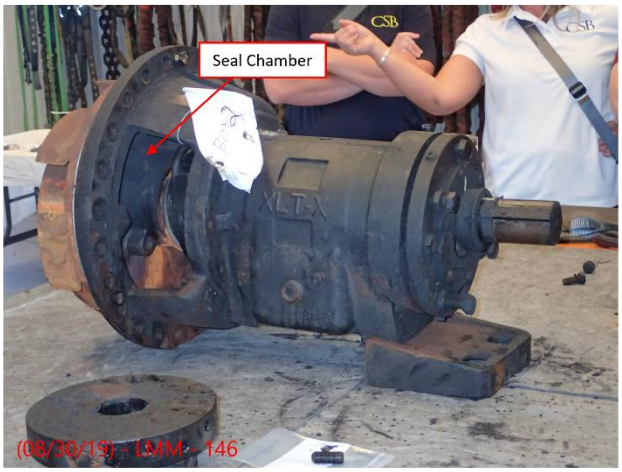

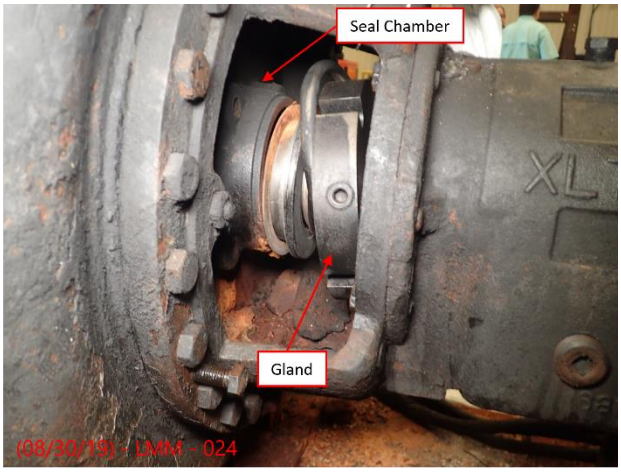

Fig. 2 – Seal Chamber Assembly Showing Detached Gland

Figure 2 shows the ultimate component failure in the pump assembly which allowed for the leakage of petrochemical product which lead to the fire. There is clear separation of the glad from the seal chamber.

Fig. 3 – Seal Chamber Closeup, Alternate Angle

The angle of the seal chamber and how much the glad has been detached from where it should mate with the seal chamber face in Figure 3 shows the extreme results of components working themselves apart. There is only one stud remaining to hold the gland to mate with the seal chamber, the remaining three have come loose.

Fig. 4 – Exemplar Seal Chamber

In contrast to how the assembly should fit together shown in Figure 4, the detachment is even more glaring, with the surfaces that would normally be clearly aligned and fixed together by the clamping force of the nuts on the seal mounting studs at a significant angle out of perpendicular with where they should be.

Fig. 5 – Bearing Housing with Loose Ball Bearings

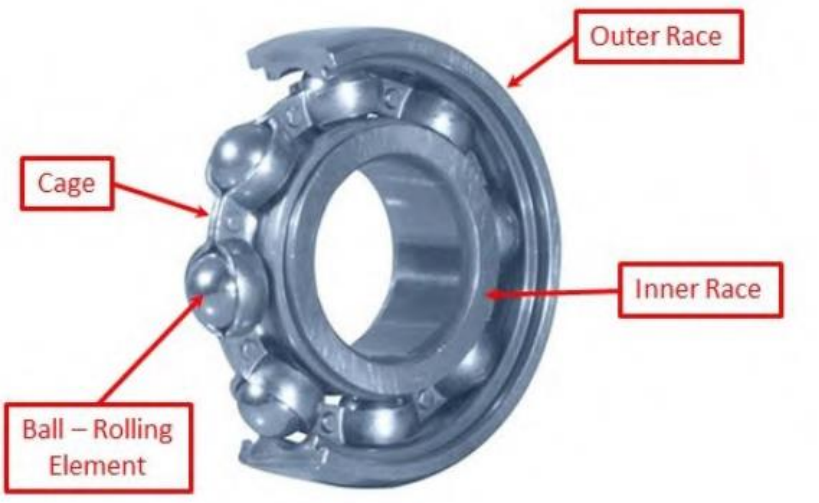

Fig. 6 – Bearing Diagram

When taking Figure 5 and 6 together, it is clear there is systematic failure of the bearing assembly for the outboard bearing of the pump. The cage which would ordinarily confine the ball rolling elements and keep them spaced is no longer either visible or performing its intended function.

Fig. 7 – Outboard Bearing Race

Fig. 8 – Outboard Bearing Balls

As shown in Figure 7 the outboard bearing race has significant buildup of debris and residue from bearing wear. The bearing balls in Figure 8 show significant plastic deformation and oxidation as well as a large variance in size, potentially due to long term wear.

Fig. 9 – Bearing Ball with Void

The damage on this bearing balls appears to be primarily due a partial melting of the ball's material and a layer of oxide covering the entire component. There is substantial void in the center of this one shown in Figure 9.

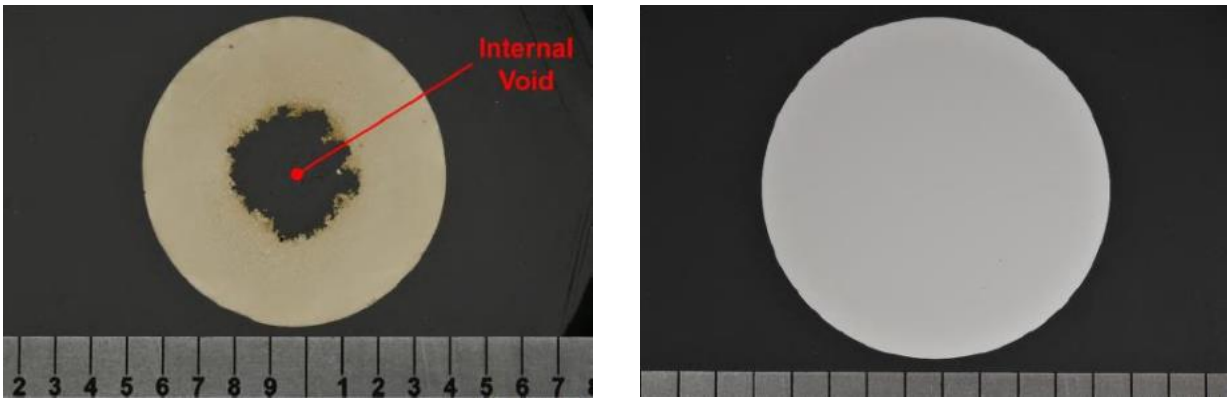

Fig. 10 & 11 – Bearing Balls with Internal Void and Normal

Figures 10 and 11 taken together show the substantial damage and loss of material the bearing balls in the subject pump had inflicted upon them.

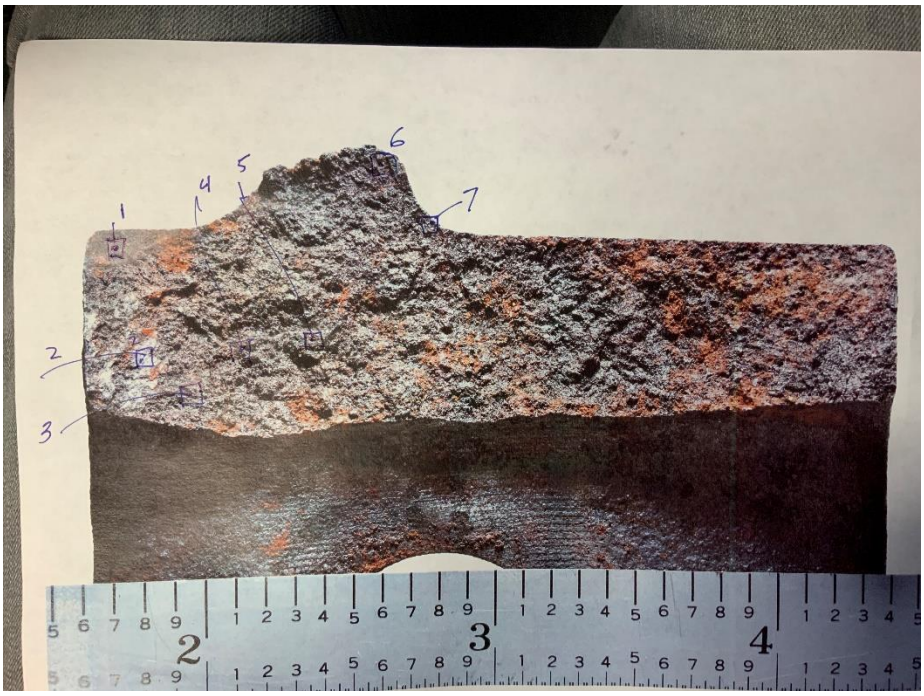

Fig. 12 – Pump Foot Fracture Surface with Numbering for SEM Analysis

The fracture surface of the pump foot in Figure 12 shows significant oxidation, validated by results from spectrometry across the surface. Much of the oxidation is not what would be expected if it oxidized exclusively during the post failure flames, lending to the conclusion that at least some parts of the surface had been exposed to to the elements prior to the incident.

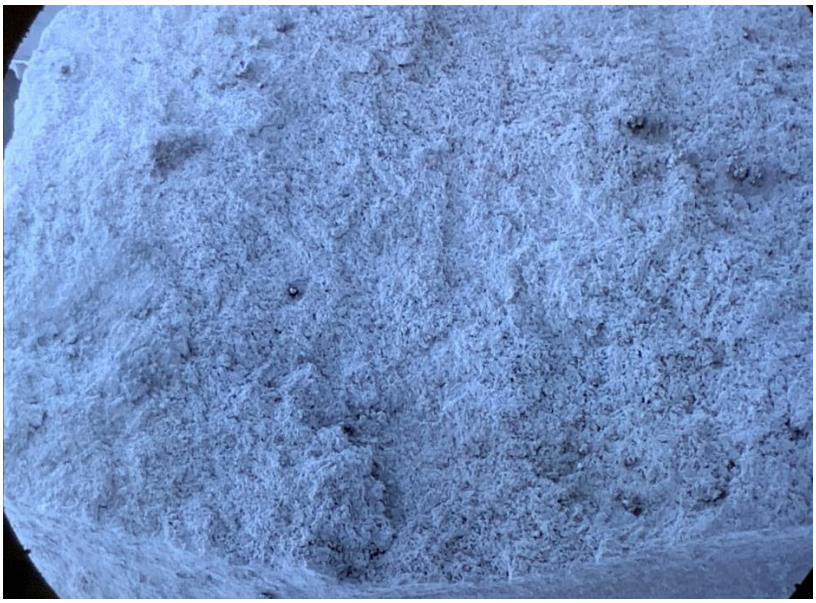

Fig. 13 - Fracture Surface at Location 4

SEM investigation of Location 4 on fracture surface of pump mounting foot shows evidence of brittle, fast fracture with intergranular fracture characteristics. There are no obvious signs of long-term fatigue, plastic deformation caused by a fracture front's propagation or time variant oxidation from long term exposure while a crack formed. The area which does appear to have plastic deformation, potentially a result of the long-term fatigue of this component.

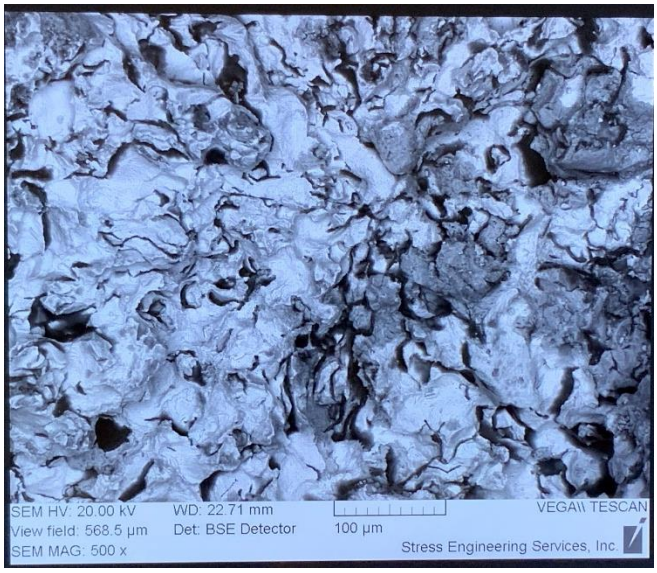

Fig. 14 – Fracture Surface at Location 6

The SEM imaging done in Figure 14 foot's shows a quite different surface to that in Figure 14. There appears to be larger scale material flow and solidification, potentially as a result of the area getting to melting temperatures in the fire after initial failure.

Fig. 15 – Pump Foot Bolt Mounting Hole

The installation of the pump at the feet and its fixturing to the ground shown in Figure 15 is a major point that raises a flag. From the information given the pump feet where not anchored

to the ground to a specified torque to attempt to minimize the possibility of movement and vibration. The fact that these bolts were not installed to a designed and specified torque does not appear to be the outcome of installers not meeting the standards set in the owner's manual, as no torquing information is included in the owner's manual for the pump and the only instruction is to hand tighten the bolts. The manual does go in depth on the I-procedure and importance of leveling and alignment of the pump sections to prevent elevated wear and stress on components. It does not even include a maintenance regime that would result in the prevention of failures due to a lack of lubrication or alignment of shafts. It is possible that if all other operations are followed, hand tight is enough.

Potential Failure Mechanisms

The following failure mechanisms are possible given some portion of the evidence and will have their merit discussed:

1. Fatigue from erroneous dynamic stresses allowed in the system from improper installation and maintenance
2. Inadequate alignment and leveling at installation allowed movement which lead to off axis loading of shaft, bearings, pump mounting feet, and seal studs leading to galling of threads/shafts and hot plastic flow of bearing balls under elevated temperatures resulting from the increased friction in this load case
3. Seal itself was not manufactured to specifications and came loose due to
4. Corrosive environment led to accelerated fatigue of pump mounting feet first and after fracture at that location the whole assembly came out of alignment and underwent adverse loading conditions culminating in ultimate failure of seal

We do know that the inspections required by the owner's manual on a regular 3-month schedule were not conducted and much of the wear present on the parts under investigation would have shown clear signs of deterioration so improper maintenance does play a factor but is unlikely to be the whole story.

There appears to be sufficient evidence that at least at one point in the process of the subject pump failing there were issues with alignment. With fractured mounting feet which are ordinarily used for locking in adjustments made to alignment, I am comfortable with accepting

there were alignment issues but I have a hard time accepting that this was in isolation the only factor in failure. The coupler allows for a few degrees of variation and just from the evidence presented to me I do not know if it fell outside of it. However, there are failures which point to erroneous loading which could line up with this if the misalignment was sufficiently large enough.

While it is possible that the parts which were installed in the pump assembly are not withing specification, it is unlikely that it would have taken as long as it did for this failure mechanism to result in a leak of product. If this part did not fit or was unable to adequately transfer/accept loading in these conditions, then it would have been apparent immediately and not after enough time for many other components to corrode and fail the way we see. This would not be expected to assist in the fracture of the mounting feet as well, which is in my opinion an important part of the progression of this failure.

The types of oxides present on the surfaces of parts proves that a corrosive environment did exist. However, on several key parts it is not clear whether that is something which contributed directly to weakening the parts in the ways necessary to cause them to fail alone assuming design loading conditions.

I believe that a confluence of the listed potential mechanisms is responsible for the failure of the pump system in the way that it did.

Conclusion

From the investigation conducted, the mechanism of failure is likely to by a combination of downstream secondary factors stemming from inadequate anchoring of the pump to its slab and inadequate maintenance and inspection compounding the issue. As the pump worked itself loose and the anchors were no longer capable of holding the pump in place, the two sides of the pump mechanism, coupled in the center, began to come out of alignment and created a bending moment on components not designed to manage that form of loading. This led to an increase in friction between parts and a rise in temperature as a result. This rise in temperature outside of the design temperature of the pump led to a number of intermediate failures. These failures include a

loss of operating clearance in several locations including the pump itself where the impellor wore into the housing, the bearings where significant damage to both the bearing balls and the tracks alike. Once clearance in these parts was lost, more heat was created potentially resulting in lubrication failure, increasing the potential for galling of components which began coming in contact with one another, and eventually beginning to melt the bearing balls in a catastrophic failure of that assembly.

References

Tallian, T. E. (2003). Chapter 13: Heat Imbalance Failure. In *Failure Atlas for Hertz Contact Machine Elements*. essay, ASME Press.

STARFORGE DESIGN REPORT SUMMARIZATION

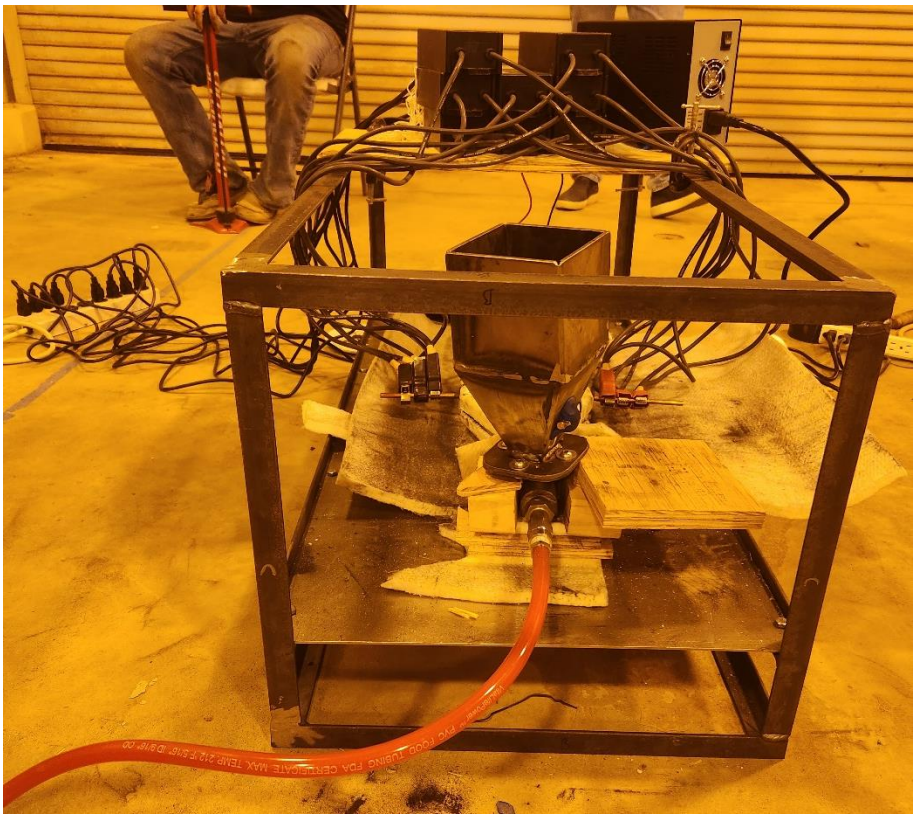

05/02/2023

EXECUTIVE SUMMARY

In-situ resource utilization (ISRU), or the ability to access raw materials in space, has been identified as a necessary step in NASA's goals of establishing permanent and sustainable human presence in space. However, while the materials necessary for everyday human life are abundant in space, the processes used today to extract and refine them into useful material are far too heavy and complex to be transported directly into space. There remains a need for an effective method of processing raw materials found on celestial bodies which does not require the expensive transportation of complex and heavy chemical processing equipment or large infrastructure for traditional material extraction techniques. The absence of such a process provides an opportunity to revolutionize the space mining industry and unlock its significant scientific and commercial potential. A process which utilizes a gliding arc plasma-assisted reactor to separate the chemical bonds in metal oxide compounds was designed, followed by a particle accelerator and mass sorting system to extract, and isolate the desired metals. Notably,

this process can operate continuously, further improving efficiency and reducing cost. In addition to this, this concept has the potential to run completely from materials readily available at an off world mining site, leading to self-sustainability in space. A prototype was constructed with a 2400W gliding arc reactor system along with a hopper for introduction of material and the aforementioned mass sorter. The power input was achieved using eight neon sign transformers (NSTs) in parallel with two conventional 110V outlets, and the gliding arc was created using two custom graphite electrodes. A black iron oxide and charcoal mixture was introduced to a carbon dioxide working fluid using a venturi pump in combination with a hopper, was passed through the reactor. Then, any ionized material was sorted using an ion accelerator and faraday cup. The system was successful in yielding ionized material from an iron oxide-charcoal mixture, though the exact chemical identity of the material has not yet been tested. An independent mass spectrometry or chemical process is required before proving successful yield of pure iron from the input material. This design along with its proof of concept in prototyping has the potential to serve as the starting point for a vital method to enable cost-effective ISRU in support of permanent human presence in space, while showing promising applications in the metal processing industry on Earth.

PROBLEM

Problem Statement

The main problem the project is involved with is providing infrastructure/support for a currently non-existent industry in a sustainable way. This problem is challenging to solve due to the minimal existing technology and market/industry for this field. Those involved in and benefiting from resource extraction and scientific endeavor will benefit from the solution to this problem. The current state of off-world resource acquisition operations is strictly research based in which samples are gathered and sent back to earth for testing and analysis. This clunky and expensive process must be revised and built upon to ensure proper development and success of off-world resource extraction for the advancement of space exploration and industrialization. This will necessitate in-space production and the acquisition of critical resources to fuel necessary supply chains to an entirely new standard to solve the problems of efficiency as well as capability within an untapped and innovative industry.

Motivation

This problem is important due to the Earth's heavy reliance on native gathering and refinement processes of natural resources. According to the National Footprint and Biocapacity Accounts, "Humanity is using nature 1.8 times faster than [Earth's] biocapacity can regenerate."(HME, 1) This correlates to the current trend of industrialization of humanity to be significantly unsustainable. This will eventually result in drastic damage to the planet, jeopardizing infrastructure, and humanity entirely. This issue is further compounded with the increased need for rare earth elements due to massive potential within renewable energy. Although these benefit renewable methods, the overall resource requirement of these methods are significantly greater than the polluting counterparts. According to Harvard international review, "an electric car requires six times the mineral inputs of a conventional car," as well as "a wind turbine requires nine times more minerals than a gas-fired plant." (Nayar, 1) Therefore, the ability to alleviate this continued and increasing strain on the earth's natural reserves is paramount in maintaining sustainability to continue as an advanced civilization.

Function

Our design works by developing a gliding arc discharge in our reactor to supply a low temperature, low pressure carbon monoxide plasma in stream with microparticles of metal oxide This supplies the energy and environmental conditions necessary for an efficient redox reaction, in this case producing pure iron Fe^{2+} and CO_2 as products. Iron ions are then picked out of the flow and collected on a negatively charged Faraday Cup which supplies the ion with its missing electron and stabilizes it enough to stay attached (application of technology which enables mass spectrometry) Carbon Dioxide is then discharged from the system as a byproduct which, in the context of processing off world, does not have adverse effects. The primary means of validation of a successful operation is by measuring the mass change of the faraday cup as well as visual inspection to confirm that the compound was successfully separated and processed.

Innovation

		Concepts			
	Laser Ablative Mining	Spark Ionization	Spark Ionization (Traditional)	Thermal Ionization	Gliding Arc Reactor

		(Continuous)			
Energy Efficiency	Datum	+	S	-	S
Compatibility		S	S	-	+
Maintenance		-	S	-	+
Technical simplicity		-	+	S	-
Ease of transport		S	S	-	S
Power input		+	+	-	-
Volume		S	S	-	+
Internal pressure		S	S	S	+
Process efficiency		+	S	+	+
Thermal insulation		S	S	-	S
# Of Pluses		3	2	1	6
# Of Minuses		2	0	7	2

Fig. 4 Concept Evaluation Pugh Chart

From Figure 4, the gliding arc reactor design outperforms the other three design choices through its innovative ionization technique. The gliding arc design enables the temperature to reach 12000K within the reactor with 70kW/m of power input. This reactor is much smaller than the other designs, only reaching a length of 12 inches. Finally, the length of the electrodes, as shown above, can be adjusted to increase total arc power with the length.

The extraction of pure elements usually occurs one of four ways. Solvent extraction, distillation, pressing or sublimation. Our team introduced an alternative to these methods by using

a gliding arc to create a potential difference between two electrodes. While electricity is commonly used in industry to sort refined material our design implements it by ionizing raw material and kickstarting a secondary combustion process between CO2 and iron oxide.

REQUIREMENTS

Overview

With rapid industrial growth in space there is a need for more efficient material processing methods, which our design fulfills using an innovative gliding arc reactor and electromagnetic sorting system combination.

Design Requirements

- Must Do
    - Must intake material and introduce it to a fluid flow
    - Must prosses material in a gliding arc reactor creating ionized particles
- Should Do
    - Should separate out ionized particles electromagnetically based on their atomic weight
- Could Do
    - Could control ratio of material to working fluid using a vibration motor to agitate a hopper
    - Could measure temperature of reaction

Engineering Requirements

1. Power Input of at least 1,200 W
2. Volume of 3 cubic feet or less
3. Internal Pressure 275,790 Pa
4. Process efficiency of at least 5%
5. Thermal Insulation (K/W)

The engineering requirements listed above provide the overall parameters for the general processing product design. The required and limited power input for the system is 3600W that are provided by to 120V or one 240V outlet.

DESIGN

Computer Aided Design

Autodesk's Inventor Pro was used to design components and create assemblies of the full design. Figure 7 shows a fully assembled model of all components the team designed and produced. This includes the sub-assemblies for the support structure, inlet and outlet systems, reactor system, and sorting system.

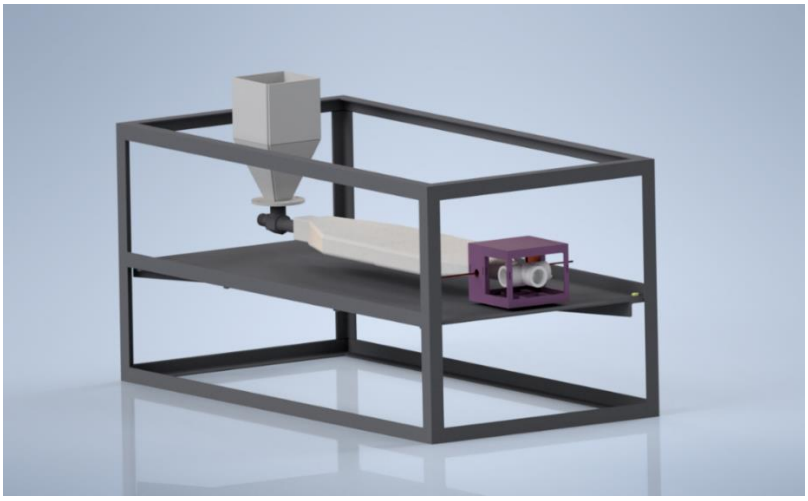

Fig.7 – Full Design CAD Model

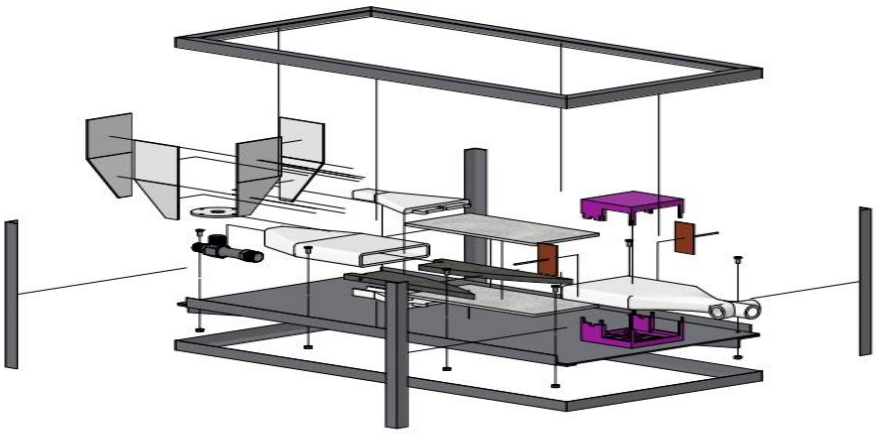

Fig. 8 – Full Design CAD Model (Exploded View)

The exploded view of the assembly (Fig. 8) shows the fitment of individual components of the design. Steel components were welded or bolted together, while all other components were press fit.

Fig. 9 - Electrode Design

Shown in Figure 9 is the design for the gliding arc electrodes. The electrodes served as the core of design and are essential to the function of the gliding arc reactor system.

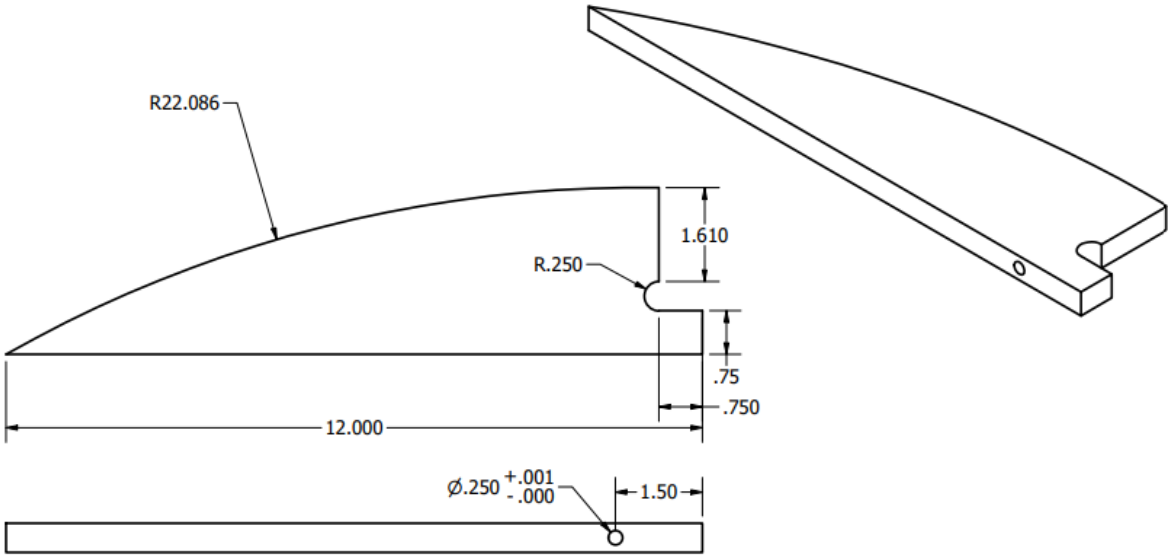

Fig. 10 – Dimensional Electrode Design

The geometry of the electrode shown in Figure 10 was designed to allow for a discharge of electricity across a CO2 plasma that develops various phases of power transmission characteristics along the length of the reactor as the fluid flow of CO2 and entrained iron oxide move through the system and expand. A blind hole is added to allow for electrical connections to be attached. Radiused indexes at the base are used to align the reactor and allow for the electrode to be manufactured on a CNC Mill.

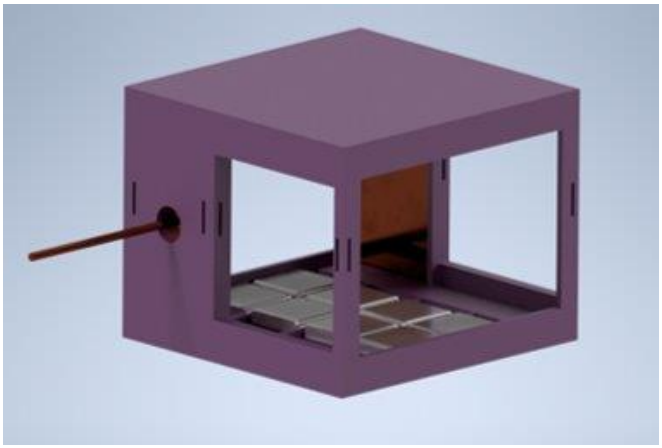

Fig. 11 – Sorting System Design

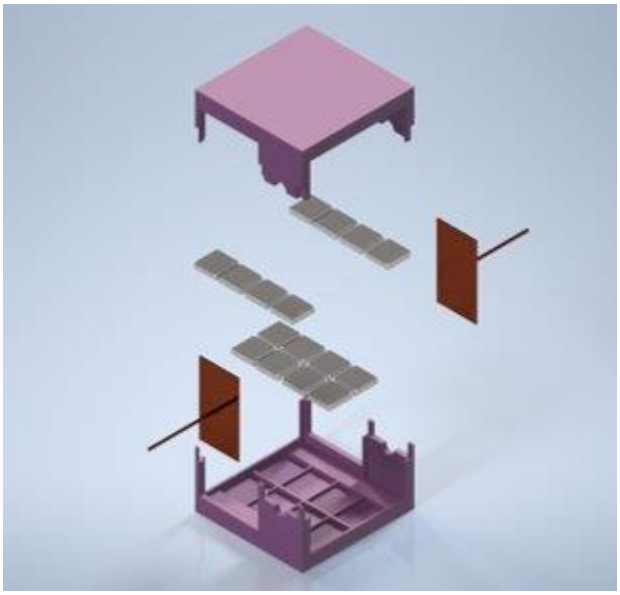

Fig. 12 – Sorting System Design (Exploded View)

The sorting system shown in Figure 11 and 12 was designed with a 3D printed housing, neodymium magnets, and copper plates to facilitate ion acceleration and sorting. All components were press fit and secured with JB weld.

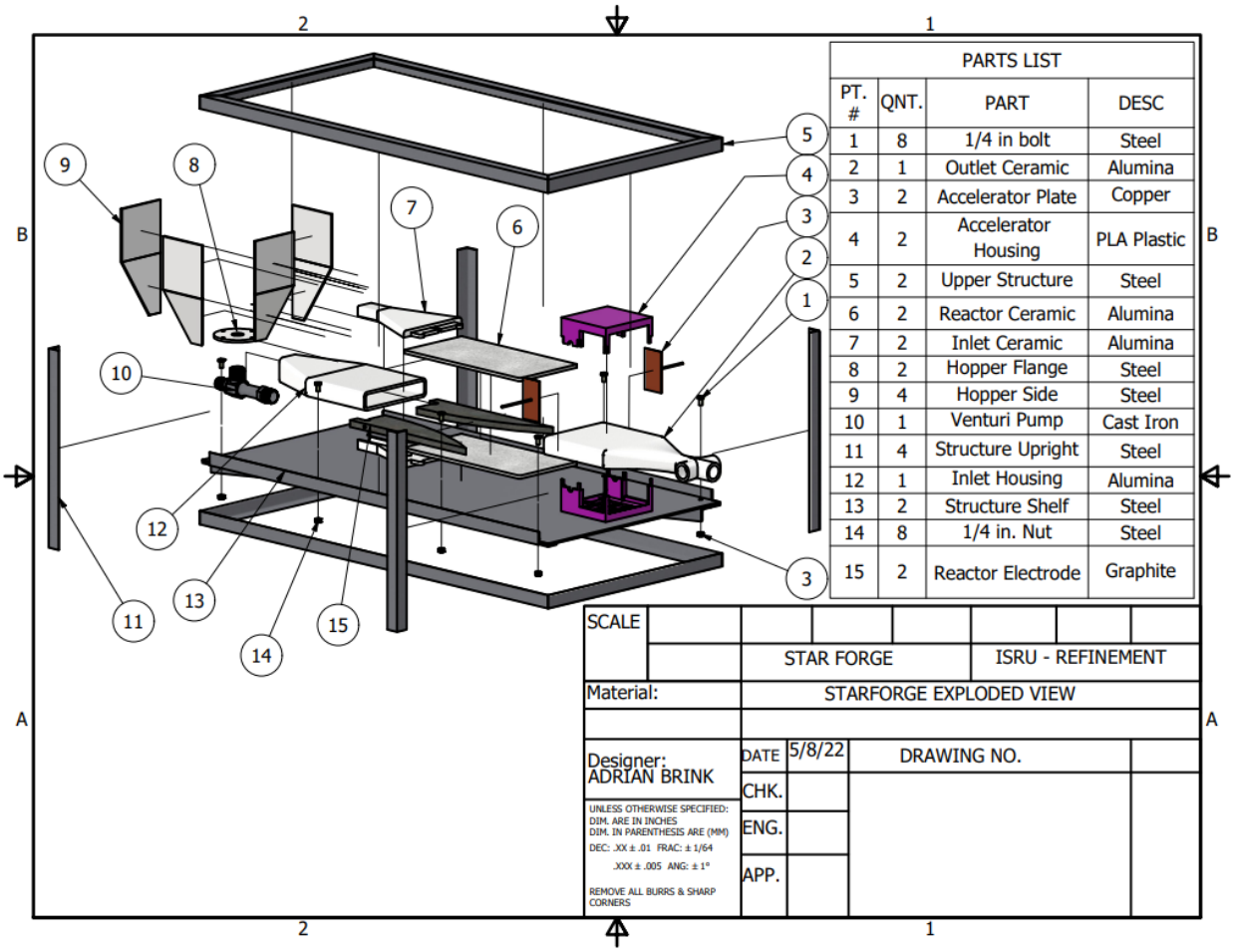

Fig. 13 - Exploded View (With Parts List)

All parts included are in reference to Figure 13. The hopper section and venturi pump interface into the inlet section. The inlet section is comprised of an internal and external section as displayed in parts 7 and 12. This allows the flow to properly condense into the reactor system comprised of two ceramic tiles and graphite electrodes depicted in parts 6 and 15. The Products of the reaction are then expanded and separated by the outlet section and sorting system respectively, depicted in parts 1 through 4. The structure to properly fixture the system is observable in parts 5, 11, 13.

Fig. 15 – Manufacturing Gantt Chart

Manufacturing

Hopper- The hopper was manufactured by plasma cutting 4 sections total of 1/8th inch steel. 2 of the sections were for the angled section of the hopper while the other two were for the straight upper sections. Each respective section was ground along a seam to 2/3rds of its original thickness and then bent in a sheet metal finger brake. These now bent sections were then fixtured and welded to create the final assembly of the hopper. Next, flanges were also plasma cut from the 1/8th inch steel and face milled to the correct thickness to properly accept the nylon mesh. One flange was directly welded to the hopper while the other flange was welded to a ¾ NPT nut to allow interface to the venturi pump and hopper with the flanges bolted together.

Inlet – The inlet section was comprised of internal and external sections using refractory alumina cement as the material. Both sections had to be manufactured using molding techniques from 3D printed molds. The internals mold was designed to be a traditional two-piece cope and drag designed mold with the use of ejector pins to allow for easy and consistent parting of the finished part from the mold. The exterior mold was designed to be a three-part mold with an open

end to allow for the molding material to be poured in to fill the negative space created by the center part of the printed mold. The mold is then disassembled and parted from the finished part.

Reactor – The reactor was created from low porous graphite plates. The plates were then cut using a CNC mill configured using specific geometry from our CAD models. The relatively complex geometry of the electrode in combination with the brittle nature of graphite made manufacturing challenging. The CNC mill provided the most precise and careful manufacturing method and minimized the risk of lost material. In addition to using the CNC mill we created a metal brace to secure the graphite and minimize vibration that could produce excess stress on the electrode during cutting.

Outlet – This section was manufactured using 3D printed molds through investment casting techniques. Our molding material, Alumina refractory cement, was mixed and poured into our mold. Due to the complexity of the mold, we cast in two sections. After the first section was cast, we applied the second mold housing and filled. Our mold was then left to dry for 24 hours and then removed from the housing. At this point, we placed the mold into an oven at roughly 400 degrees Fahrenheit to melt out the internal 3D printed section. This process removed our unwanted PLA in the internal mold section while drying and hardening the refractory surrounding it. While the oven removed the bulk of the material, spot heating and melting was done in small sections of the outlet using a blowtorch.

Particle Accelerator – The particle accelerator was created from a 3D printed housing with built in recessed sections to hold neodymium magnets. The magnets were then held in place and sealed by an epoxy resin. The sides of the particle accelerator also held copper plates with wired leads which would be connected to an external power supply.

TESTING

Testing Plan

Electronic systems were first tested without flow to verify parallel transformer set up and system safety (Fig.16). This test was used to ensure our power delivery system was sufficient to create a plasma arc. This test was conducted with and without ceramic plates to observe how the arc would react in different conditions.

Fig. 16 – 900W power test

The next test exercised introduced flow between the electrodes. (Fig. 17) The flow introduced at this stage was simply pressurized air, but this observation of how the plasma arc would react was performed. From this test we could observe the length of plasma development to see if we required more power for the system.

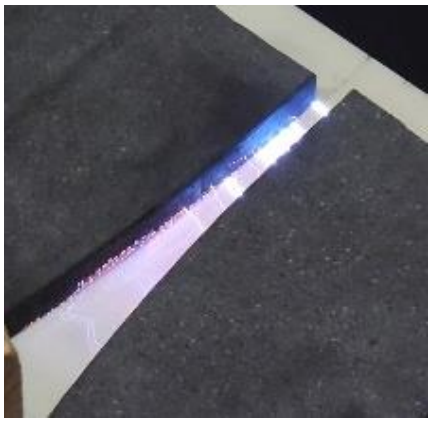

Fig. 17 – 900W Gliding Arc with Compressed Air

The next test performed changed the working fluid from pressurized air to CO_2 and introduced our raw material in the form of iron oxide (Fig. 18). As shown in figure 14 the plasma arc under actual conditions closely resembles the test with pressurized air. The change in color is due to the introduction of iron oxide and shows a successful result of our combustion reaction.

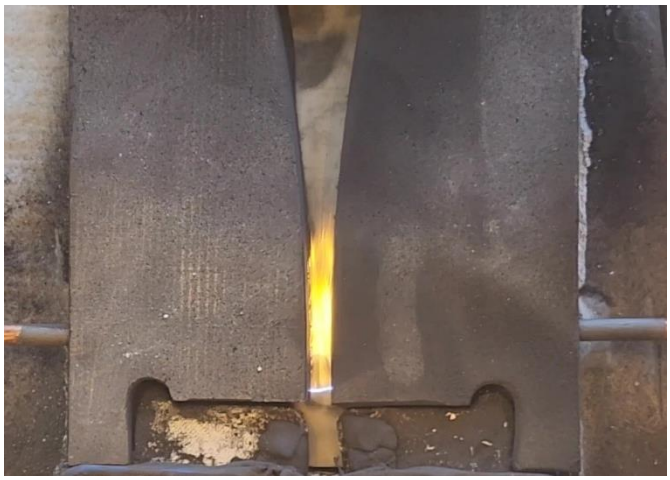

Fig. 18 - 2400W Gliding Arc with CO2 and Iron Oxide Combustion Test

The final test was a full assembly test. The particle accelerator and venturi systems were added, and the system was run continuously for 30 minutes. The power supplied to the system was also increased by adding transformers from 3 to 8. The reactor system is fully enclosed in our ceramic housing and rested in a steel cage simply used for ease transport and structural support.

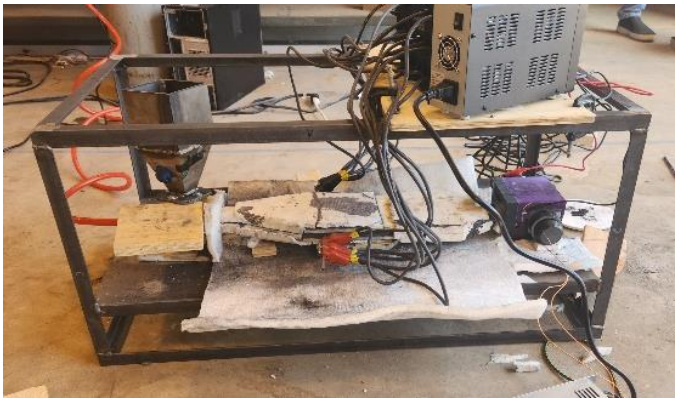

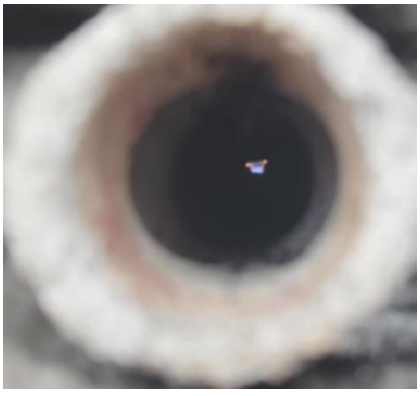

Fig. 19 - Half Hour Test of Closed Assembly (Left), Fig. 20 Enclosed Gliding Arc (Right)

Testing Results

The faraday cup yield shown in Figure 21 was observed after the 30-minute demonstration test. This yield was proven to be ionized as no material was in a neutrally charged cup placed on the opposite side of the outlet section and attracted to the faraday cup, eliminating possibility of the material entering the cup by fluid mechanical means.

Fig. 21 Faraday Cup Yield

IMPLEMENTATION

Final Design

The final implemented design (Fig. 22) utilized a hopper and venturi pump to introduce iron oxide and a charcoal additive into a CO2 flow (Fig.23). Analysis was performed to establish efficacy of the venturi pump for this specific application, resulting in an overall velocity ratio 5.42 CO2 to Iron Oxide (see Appendix A). This ratio was in turn sufficient for the process. The

integrated flow was then passed through a gliding arc reactor (Fig. 24) to produce ionized iron atoms which are then separated and collected in a faraday cup using electromagnetic properties of the element (Fig. 25). The design was powered by eight neon sign transformers in parallel, totaling 2400W of total system power minus some inefficiencies.

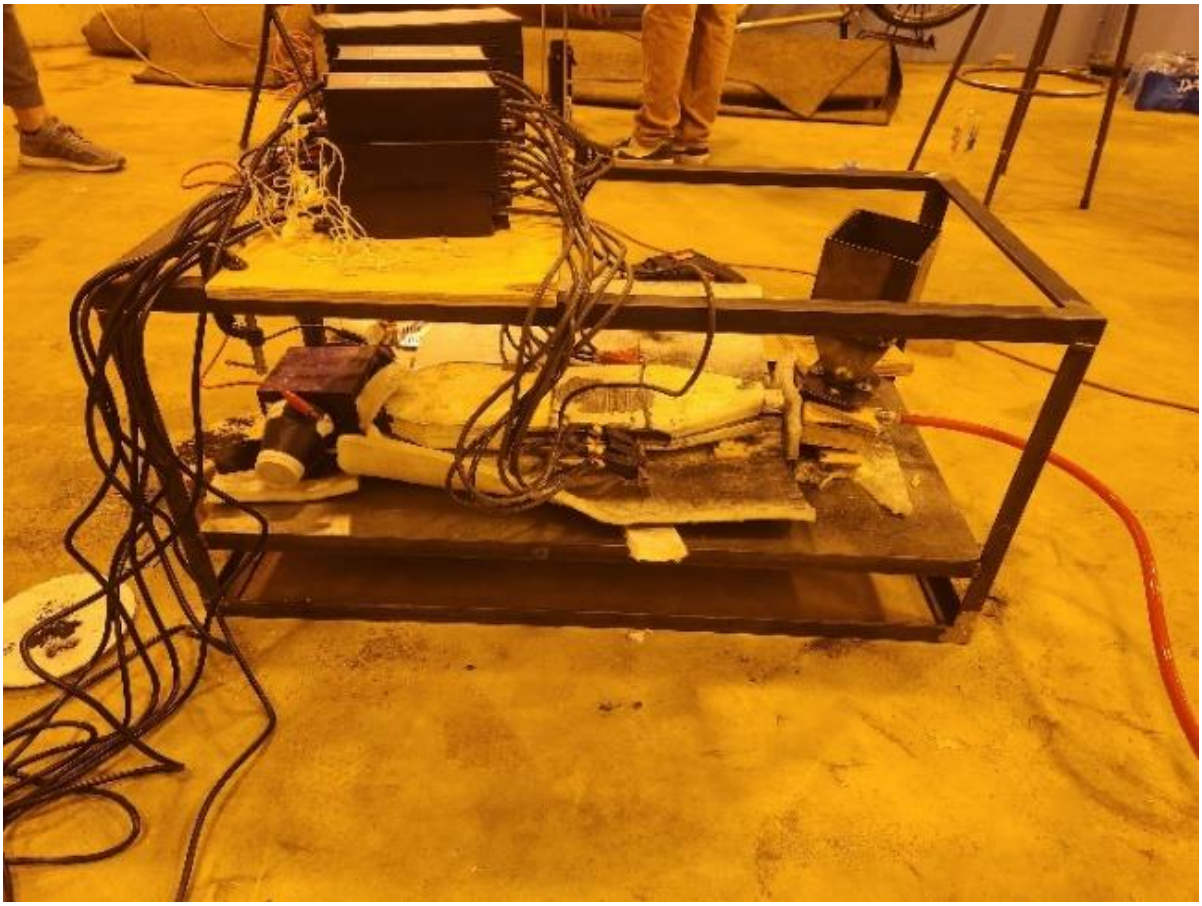

Fig. 22 - Final Assembly

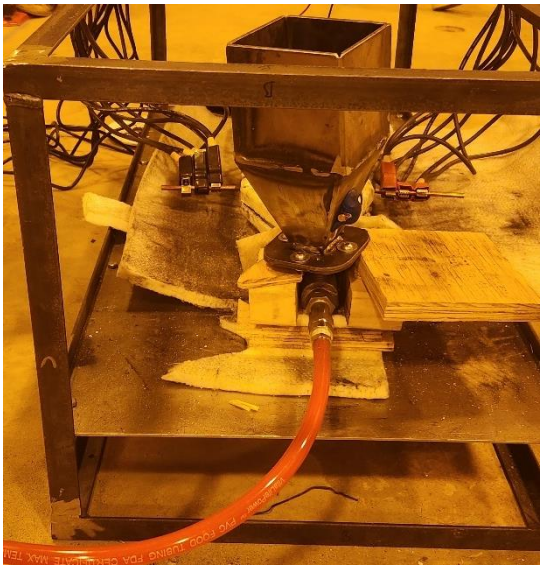

Fig. 23 - Hopper and CO2 Inlet with Venturi Pump

Shown in Fig. 23, CO2 and iron oxide were introduced to the system with a charcoal additive by stirring the material in the hopper. A fine filter was used to separate out any contaminants or material not to specifications.

Fig. 24 – Gliding Arc Reactor Section

The reactor (Fig.24) was created with two custom graphite electrodes to facilitate gliding arcs. The reactor body was cast in ceramic and then surrounded by a thermal and electric insulative blanket.

Fig. 25 - Sorting System

The sorting system (Fig. 25) utilizes an electric field and a magnetic field to produce Lorentz forces to accelerate the ionized product from the system reactor and divert it radially from the outlet flow. 16 units of one inch by one inch neodymium magnets are placed across the bottom and the top of the system, eight on each side, oriented in the same direction to produce a continuous magnetic field across the length of the sorting system. Two copper plates are placed along the length of the intake half of the sorting system, parallel to each other and perpendicular to the magnets. An 11V DC potential difference is placed between the plates to produce an electric field perpendicular to the magnetic field. When the ionized reactor products enter the sorting system, they are accelerated linearly by the perpendicular magnetic and electric fields. When the electric field drops off, the products are diverted radially by the magnetic field into the collection Faraday cup. The Faraday cup is made from a graphite crucible inside a steel pipe segment, with a 48V DC potential difference placed between the two such that the negative lead is connected to the graphite crucible. This produces a negative charge bias in line with the ion flow, attracting and neutralizing the positively charged iron product. A cup with zero net charge was placed on the opposite end of the sorting system to ensure all material was being correctly diverted by the electromagnetic system.

Fig. 26 - Power Delivery System

The power delivery system (Fig. 26) was constructed using eight 10kV 30mA transformers with their secondaries wired in parallel to combine their current and overall power. The system operated off of two 110V conventional wall outlets and delivered 2400W of power to the gliding arc reactor.

Design Assessment

The design and prototype proved the concept of using a gliding arc to process input material. The efficacy of the concept of a gliding arc assisted mineral refinement process is affirmed due to the results of the testing. This demonstrates potential for scaling and perfecting the process through integration of better resources as well as further testing and analysis. Therefore, this prototype is the first step to solving the problem of a non-existent infrastructure within space due to over encumbered, expensive, chemical-based processes that this process and design solves entirely.

Recommendations

For the future, the team recommends finding a new method to increase the potential difference and wattage of the power delivery system, as the current method of parallel neon sign transformers is limited to 3600W and was proven to be unreliable in its function. Another recommendation is to investigate the utilization of a gliding arc Plasmatron method instead of using a two-dimensional gliding arc for material processing. In terms of the flow system, better

sizing of the venturi pump is necessary to allow for better mixing ratio of materials to create a more efficient reaction. From analysis of the venturi pump found within Appendix A, the ratio of Iron-oxide and Carbon Dioxide is static and independent of flow conditions. Finally, more development for the motor to agitate input material is required to facilitate more accurate introduction of iron

CONCLUSION

The main problem the project is involved with is providing infrastructure/support for a currently fledgling industry in a sustainable way. This project presents a solution through its innovative gliding reactor creating a potential for processing more off-world material at a lower cost in weight and manufacturing. Through our design process we have considered our market, requirements for our design, requirements for our customers and compared and weighed the importance of those factors against one another. We explored and compared existing technology, researched, and improved upon our own designs and then modeled, and analyzed those designs and selected materials based on those models and created a plan for manufacturing as well as a timeline for completion. A prototype was constructed with a 2400W gliding arc reactor system along with a hopper for introduction of black iron oxide. The system was successful in yielding ionized material from an iron oxide-charcoal mixture, though the exact chemical identity of the material has not yet been tested. An independent mass spectrometry or chemical process is required proving successful ionization and yield of pure iron from the input material. Through this process we have gained the confidence that we will be able to create the best version of our solution possible and one that is worth pursuing in the future. This project should be continued as it is a potential jumping off point for future off world mining endeavors with its use of unique ionization and processing techniques.

REFERENCES

Fridman , A., Nester, S., Kennedy, L., Saveliev, A., & Mutaf-Yardimci, O. (1999). Gliding Arc discharge (thesis). Progress In Energy and Combustion Science, Chicago .

“How Many Earths? How Many Countries?” *Earth Overshoot Day*, 9 Aug. 2022, https://www.overshootday.org/how-many-earths-or-countries-do-we-need/.

Maibusch, R., Kuss, H.-M., Coedo, A. G., Dorado, T., & Padilla, I. (1999). Spark ablation inductively coupled plasma mass spectrometry analysis of minor and trace elements in low and high alloy steels using single calibration curves. *Journal of Analytical Atomic Spectrometry*, *14*(8), 1155–1162. https://doi.org/10.1039/a901650c

Nayar, Jaya. "Not so 'Green' Technology: The Complicated Legacy of Rare Earth Mining." *Harvard International Review*, Harvard International Review, 12 Aug. 2021, https://hir.harvard.edu/not-so-green-technology-the-complicated-legacy-of-rare-earth-mining/.

Recent advances in Analytical Spark Source Mass Spectrometry. (1982). *Philosophical Transactions of the Royal Society of London. Series A, Mathematical and Physical Sciences*, *305*(1491), 509–519. https://doi.org/10.1098/rsta.1982.0048

Sanders, G., & Kleinhenz, J. (2022, May 3). *In situ resource utilization (ISRU) envisioned future priorities - NASA technical reports server (NTRS)*. NASA. Retrieved June 13, 2022, from https://ntrs.nasa.gov/citations/20220004617

Sanders, G. (2021, October 3). *In-situ resource utilization (ISRU) capability roadmap final report*. Academia.edu. Retrieved June 15, 2022, from https://www.academia.edu/55111640/In_Situ_Resource_Utilization_ISRU_Capability_Roadmap_Final_Report